1. INTRODUCTION

Flow and heat transfer due to free convection and mixed (free and forced) convection are often encountered in engineering systems, *eg.*, doubly glazed windows, production of float glass, food processing, growth of crystals, solar ponds, dynamics of lakes and thermal hydraulics of nuclear reactors. The simplest configuration approximating some of these practical flow situations is the flow and heat transfer in a rectangular cavity where the flow is induced by a shear force resulting from the motion of the upper lid combined with the buoyancy force due to the heating of any of the other three plates forming the cavity. Simple geometry, unambiguous flow boundary conditions and recirculating flow with multiple vortex formation have justified the use of the problem of lid-driven cavity without thermal effects as a work-horse problem for validation of CFD algorithms against other benchmark computation [Ghia *et al* (1982)] and measurement data [Koseff *et al* (1983)]. On the other hand, the free convection of a viscous fluid in a differentially heated cavity with two opposing walls held at different temperatures provides another simple problem, studied extensively by researchers [Vahl Davis (1983), Wan *et al* (2001)] to understand the interaction between buoyancy and shearing forces in such flow situation. In case of mixed convection problems when both the lid motion and the buoyancy effects due to temperature difference are present, the vortical core flow pattern is surrounded by the wall boundary layers and the average and local heat transfer coefficients (Nusselt number) are function of Reynolds number, Grashof number, Prandtl number and the cavity Aspect Ratio. Some important experimental results on mixed convection in cavity have been reported by Prasad and Koseff (1989), whereas limited computational results are reported by Xu *et al* (1998) on free convection due to bottom heating and by Moallemi *et al (*1992) and Mohamad *et al* (1993) on mixed convection situation. The flow and heat transfer characteristics for mixed convection in rectangular enclosures remains an interesting research problem for which many important aspects are yet to be explored in further details.

The present work focuses on detailed CFD analysis of flow and heat transfer in a square cavity for which the top lid wall, maintained at a lower temperature, is either stationary or driven parallel to itself at a uniform speed whereas the other three walls are stationary, the two vertical walls are thermally insulated and the horizontal bottom wall is maintained at a higher temperature. The computation of flow and heat transfer is carried out using a pressure-based finite volume type flow solution algorithm RANS2D [Majumdar *et al* (2003)], developed at the CTFD Division, NAL, Bangalore for time accurate computation of incompressible flow in complex configuration. The effect of the governing parameters on the flow pattern and heat transfer are studied in details to understand the relative role of fluid shear and buoyancy in this complex flow situation.

1.1 STATEMENT OF THE PROBLEM

Fluid flow and heat transfer are modeled in a two dimensional rectangular cavity of width L and height H in which the top lid surface moves across the cavity from left to right at a constant speed U_L, as shown in Fig 1.1. The vertical walls of the cavity are insulated and the top and bottom surfaces are maintained at constant temperatures T_C and T_H , respectively, with $T_C < T_H$. The flow is assumed to be laminar, and the fluid properties are constant except for the change of density in the buoyancy term (the Boussinesq approximation). Under the assumptions of small coefficient of thermal expansion of the fluid media, the fluid is considered to be incompressible; but the change in density can be represented using the Boussinesq's approximation as Buoyancy force = $(\rho - \rho_c)g = \rho_c g\beta(T - T_c)$ where, β is the coefficient of thermal expansion, T is the local temperature, T_c is the reference temperature at which ρ_c is defined as the density of the fluid and g is the acceleration due to gravity. The effect of buoyancy force is introduced as an additional source term in the momentum equation along the vertical direction. The non-dimensional parameters which decide the flow pattern and heat transfer in a rectangular cavity due to mixed convection are Reynolds number (*Re*), Grashof number (*Gr*) and Prandtl number (*Pr*), defined as flollows

$$Re = U_{ref} L_{ref} / \nu , \quad Pr = \nu/\alpha , \quad Gr = g\beta(T_h - T_c)L_{ref}^{\ 3} / \nu^2$$

where, ν and α are the kinematic viscosity and thermal diffusivity of the working fluid. U_{ref} and L_{ref} are the reference velocity and length respectively for the problem considered.

The present work is divided into three different subtasks – (1) the accuracy of the flow solution algorithm used for computation is first assessed through computation of isothermal flow in a lid driven square cavity. (2) flow and heat transfer is analysed for free convection in a bottom heated thermal cavity of different aspect ratios and prediction of the critical Rayleigh number as well as the formation of the Rayleigh-Benard convection cells in cavities with aspect ratio other than unity. (3) flow and heat transfer analysis for mixed convection in a bottom heated lid driven square cavity and validation of the computation results against other computation and measurement data.

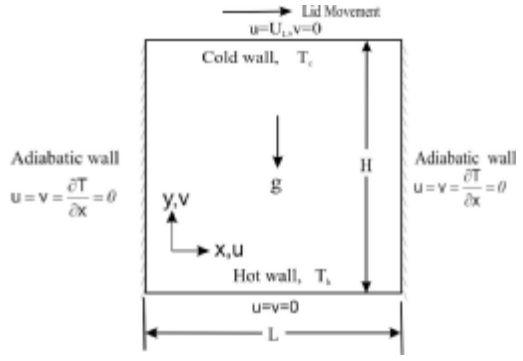

Fig 1.1 Schematic representation of a rectangular cavity with boundary conditions

2. LITERATURE SURVEY

2.1. SIDE HEATED STATIONARY CAVITY

Flow and heat transfer due to laminar free convection in a rectangular enclosure has been studied extensively during the last four decades. The research papers of Eckert *et al* (1961) or Elder (1965) published in early sixties focused mainly on the measurement of the flow pattern and the temperature field for free convective flow in a rectangular cavity with temperature difference maintained across the side walls. In Eckert's work, the temperature field in an air layer enclosed between two isothermal vertical plates with different temperatures has been investigated with the help of a Mach-Zehnder interferometer. Local heat transfer coefficients are derived from the temperature gradients in the air normal to the plate surfaces. For large Grashof numbers at a Prandtl number =0.7 and below a certain aspect ratio, the boundary layers are identified along the enclosure surfaces where the major part of the heat transfer takes place and the temperature in the central core is observed to be uniform along horizontal direction. Fluctuations in the flow and wave motions are observed in some of the measurements. Finally correlations based on measurement data are presented for the local and average heat transfer rate.

The experimental study of Elder (1965) analyses laminar free convection in a vertical slot where the aspect ratio is varied from 1 to 60 and the Raleyigh number $Ra = g\beta(T_h - T_c)L^3/\nu\alpha$ is below 10^8. For $Ra < 10^3$, the heat transfer is mostly by conduction, but a weak stable unicellular circulation is generated. For $10^3 < Ra < 10^5$, large temperature gradient grow near the vertical walls, and a uniform vertical temperature gradient is established in the interior part of the cavity. Near $Ra = 10^5$, a steady secondary flow is generated in the interior region of the primary vortex. A regular cellular pattern becomes superimposed on the basic flow to produce a 'cats eye' pattern of streamlines. Beyond $Ra = 10^6$ when the secondary cell amplitude is large, a further steady cellular motion is generated in the weak shear regions between each cell.

Rubel *et al* (1969) reports computation of flow for steady state free convection of a fluid in vertical rectangular cavity with isothermal side walls and adiabatic top and bottom walls for $6\times10^4 < Ra < 3.6\times10^5$ at Pr = 1, 6 and 2000 and at a fixed aspect ratio of 5. The governing non linear fourth order equation for the stream function and the coupled second order energy equation have been solved numerically by a stable and rapidly converging iteration scheme. The mild effect of mesh size on the flow computation results is reported and a 50 × 20 grid is considered to be adequate for prediction of the flow characteristics with appearance of multi cellular structure at an aspect ratio of 5.0. The authors conclude that unicellular flow characteristics are obtained for moderate Rayleigh number ($< 10^5$) and for the value of Ra beyond 1.2×10^5, the unicellular pattern begins to change with formation of weak central double cell and strong single cells near the top and the bottom of the cavity as well. Increase in Prandtl number leads to the formation of central cells at high Rayleigh number, but no cellular structure are observed near the top or bottom of the cavity up to $Ra = 3.6\times10^6$ and $Pr = 6$. The results suggest that strong dependence of the Prandtl no. on the flow pattern takes place at high values of Ra only.

Very important contributions in the area of computational analyses of flow and heat transfer in free convection are reported by G. de Vahl Davis (1973,1976,1983) and his research group between early seventies and late eighties. The flow field as well as the important heat transfer parameters have been computed for laminar free convection in rectangular enclosures with vertical side walls maintained at different temperature. These accurate computation results are more or less used as benchmark computation for this problem by the other researchers later. The Rayleigh number (based on the distance between the isothermal walls of the cavity) has been varied from 10^3 to 2×10^5 for a square cavity and upto 1.25×10^6 for a cavity aspect ratio of 5. It has been observed that high Prandtl numbers exert a stabilizing influence on the numerical solution, while they have only a small effect on the final results ($10^{-1} < Pr < 10^3$). Development of thin boundary layer is observed near the cavity walls when the *Ra* increases and it is well established at this stage that strong vorticity generated near the walls is able to sustain the weak return motion in the outer part of the boundary layer. Reverse flow is also observed near the center of the cavity at high *Ra* number. As far as temperature distribution is concerned, the temperature profile is virtually linear at *Ra* value below 10^3 and the heat flow across the cavity is mainly due to conduction. As *Ra* increases , the convection becomes significant and the profiles show a progressive departure from the linearity. The temperature gradient across the isothermal walls of the cavity becomes smaller showing that the amount of heat crossing the cavity directly by conduction decreases. Beyond *Ra* = 10000, the temperature gradient across the isothermal walls becomes negative and conduction in the central core of the cavity is actually opposite to the overall direction of heat flow. The horizontal temperature gradient at midpoint of the cavity becomes minimum at *Ra*~35000. However the vertical temperature gradient profile in the mid point of the cavity shows a complex behaviour. At low *Ra*, when the motion is in conduction regime ,the vertical gradient is essentially zero, As the fluid passes through the transition regime between conduction and convection, the gradient increases and experiences an oscillation with increasing *Ra*. The vital role of Prandtl number on the stability of the solution has been explained at high Rayleigh number only. Computations carried out for Prandtl number varying from 0.1 to 1000 at wide range of Rayleigh number show significant effect of *Pr* only for large values of *Ra* beyond a level of 5×10^4.

2.2 BOTTOM HEATED STATIONARY CAVITY

When the fluid is enclosed in a rectangular cavity located in a vertically downward gravity field and the cavity is heated from below instead of the differential heating of the side walls, the question of thermal stability becomes very important and many interesting findings based on classical analyses and supported by measurement, have been reported by Chandrasekhar (1961), Ostrach (1954), Benard (1900) and Rayleigh (1916). These investigations confirm that when a horizontal fluid layer is heated from below, a critical temperature gradient or a corresponding Rayleigh number needs to be exceeded before convective motion becomes established. In another research paper Catton *et al* (1967) presented systematic experimental results giving the Rayleigh number at which convection initiates in a closed cell and also the Nusselt number versus Rayleigh number relationship which prevails after convection is initiated. However their paper focused more on the effect

of the side wall boundary conditions on the free convection between horizontal plates heated from below.

Some interesting computation results on bottom heated rectangular cavity has been reported recently by Xu *et al* (1998) who used Gas Kinetic BGK scheme in the incompressible limit to simulate Rayleigh-Benard convection cells in a bottom heated cavity. Using a simple 80×40 control volume grid, the critical Rayleigh number is estimated quite accurately for a cavity with aspect ratio of 0.5. Rayleigh-Benard convection cells are also clearly observed in the predicted velocity and temperature field for aspect ratio other than unity.

2.3 BOTTOM HEATED LID DRIVEN CAVITY

Heat transfer in flows where the influence of forced convection and free convection are of comparable magnitude, are usually referred to as "mixed convection" problem in the heat transfer literature. Gebhart (1971) has separated mixed convection problem further into fluid flow and heat transfer processes pertaining to external flow or internal flows and has provided a review of some of the common geometry. Most of the experimental and numerical investigations on mixed convection process reported during the last three decades are related to external flow system, specially for general horizontal fluid layer heated from below. On the other hand internal or confined flows are of great interest to designers of alternate energy systems like solar ponds or solar storage devices etc. But very few research results are available for mixed convection in enclosures where recirculating flows are often strongly affected by buoyancy as well as the geometry.

Moallemi *et al* (1992) describes the flow and heat transfer in a square cavity where the flow is induced by a shear force resulting from the motion of the upper lid combined with buoyancy force due to bottom heating. The numerical simulations are performed for two dimensional laminar flow ($100<Re<2200$) and the effects of small to moderate Prandtl numbers ($0.01<Pr<50$) on the flow and heat transfer in the cavity are investigated for different values of Richardson number ($Ri = Gr/Re^2$) which happens to be one of the main governing parameters of any mixed convection problem. The coupling between the heat transfer and fluid flow in the cavity takes place through the buoyancy forces included as an external source term in the momentum equation along the vertical direction. The numerical solution is obtained by discretizing the governing equations using a control volume approach with the power law scheme for calculating the fluxes at the faces of the control volume. SIMPLER algorithm is used with the inertial relaxation method to accelerate the convergence. To solve the large velocity and temperature gradient in the boundary layer near the cavity walls non-uniform grid has been used along both x and y direction. The effects of Prandtl number on the flow structure and heat transfer in a cavity is found to be more pronounced for higher values of Pr, for given values of Re and Gr. The general observation is that the free convection effects always assist the forced convection heat transfer and the extent of the enhancement is a joint function of Pr and Ri.

Mohamad *et al* (1993) performed experiments to investigate free and mixed convection in shallow rectangular cavities, heated from below. Cavities with aspect ratios 1/10 and 1/5 in the longitudinal and spanwise directions respectively using Ethylene Glycol and water as working fluids for Reynolds number in the range of 170 to 2500 and Rayleigh number up

to 8.3×10^4. Flow and temperature fields are visualised using aluminium particles and liquid crystal techniques. The temperature history is recorded at different locations and 2D numerical simulations have also been carried out. Complex flow structure is predicted when, the Richardson number $Ri\ \left(=Gr/Re^2\right)$ is of the order of unity and the effect of lid motion is found to be insignificant for $Ri< 1$.

Prasad *et al* (1996) carried out an extensive experimental study of the combined forced and free convection process within a three dimensional recirculating flow in an insulated lid-driven cavity of rectangular cross-section (150 mm × 450 mm) of variable depth (between 150 mm and 600 mm) along the spanwise direction. The forced convection is induced by a moving lid , which shears the surface layer of the fluid in the cavity, thereby setting up a recirculating flow, while the free convection flow is induced by heating the lower boundary and cooling the upper one. By appropriately varying the lid speed, the vertical temperature differential and the depth, the Richardson number *Ri* for these flows is varied from 0.1 to 1000. The value of *Ri* more or less represents the relative magnitudes of forced and natural convection in a mixed convection flow. The temperature differential between the lower and upper boundaries and the depth of the cavity *H* are varied to obtain the Grashof number between 10^7 and 5×10^9 . Flow visualization using the liquid crystals and heat flux measurements at specific locations over the lower boundary provide an insight into the nature of the heat transfer process under different flow and temperature conditions. The mean heat fluxes measured over the entire lower boundary are used to compute the Nusselt number. The general conclusion from the measurement is that the buoyancy effects are significant when the Richardson number *Ri* approaches unity. For $Ri <1$, the forced convection dominates the heat transfer process whereas for $Ri >1$, the buoyancy effect dominates.

Morozov *et al* (2001) reported another numerical simulation of mixed convection of pure water in a rectangular lid-driven cavity. The influence of the lid velocity and water density extreme on convective current structure and heat transfer has been studied using the SIMPLER algorithm. The calculations are performed for three values of Grashof number ($Gr = 10^4$, 1.5×10^5 and 2×10^5) with *Re* varying from 0 to 300 at a given Prandtl number ($Pr =11.59$). At $0<Re<Re_1$ (for $Gr =1.5\times10^4$, $Re_1= 25$) the heat flux through the cell increases on account of convective current enhancement at the top part of the cavity with a relatively steady temperature distribution. The current structure changes from two to three eddies at the top part of the cell due to the top lid movement. Further increase in *Re* shows that there is intensive movement of the upper eddy and its dimensions . Also, there is decrease in current intensity in the bottom part of the cavity where the natural convection plays an important role. At $Re >66$, the forced convection plays its main role in heat transfer and the convection current structure consists of a single eddy with increase in heat flux. Here two different types of stationary solution are reported for a given *Re* depending on the initial conditions of the velocity, pressure and temperature field.

3. Governing Equations OF MOTION AND HEAT TRANSFER

3.1 CONSERVATION EQUATIONS USING FLOW VARIABLES IN PHYSICAL UNITS

The governing equations for conservation of mass, momentum and thermal energy in steady laminar two-dimensional incompressible flow in cartesian coordinate system are as follows :

Continuity :

$$\frac{\partial u}{\partial x}+\frac{\partial v}{\partial y}=0 \tag{3.1.1}$$

u-Momentum :

$$\frac{\partial\left(\rho u^{2}\right)}{\partial x}+\frac{\partial(\rho uv)}{\partial y}=-\frac{\partial p}{\partial x}+\mu\left\{\frac{\partial^{2}u}{\partial x^{2}}+\frac{\partial^{2}u}{\partial y^{2}}\right\} \tag{3.1.2}$$

v-Momentum :

$$\frac{\partial(\rho uv)}{\partial x}+\frac{\partial\left(\rho v^{2}\right)}{\partial y}=-\frac{\partial p}{\partial y}+\mu\left\{\frac{\partial^{2}v}{\partial x^{2}}+\frac{\partial^{2}v}{\partial y^{2}}\right\}+g\beta\left(T-T_{c}\right) \tag{3.1.3}$$

Energy :

$$\frac{\partial\left(\rho C_{p}uT\right)}{\partial t}+\frac{\partial\left(\rho uC_{p}vT\right)}{\partial x}+\frac{\partial\left(\rho vC_{p}T\right)}{\partial y}=k\left\{\frac{\partial^{2}T}{\partial x^{2}}+\frac{\partial^{2}T}{\partial y^{2}}\right\} \tag{3.1.4}$$

where u, v, p and T are velocities, pressure and temperature respectively in their corresponding physical units, x and y are cartesian directions.

3.2 CONSERVATION EQUATIONS IN NON-DIMENSIONAL FORM

Now if one of the cavity dimensions, either L or H , a reference velocity U_{ref} and the specified temperature difference $(T_h - T_c)$ are assumed to be the reference quantities for length, velocity and temperature respectively, the governing equations (Eqs. 3.1.1 to 3.1.4) are transformed as following

Continuity :

$$\frac{\partial U}{\partial X} + \frac{\partial V}{\partial Y} = 0 \tag{3.2.1}$$

U-Momentum :

$$\frac{\partial U^2}{\partial X} + \frac{\partial (UV)}{\partial Y} = -\frac{\partial P}{\partial X} + \frac{1}{Re}\left\{\frac{\partial^2 U}{\partial X^2} + \frac{\partial^2 U}{\partial Y^2}\right\} \tag{3.2.2}$$

V-Momentum :

$$\frac{\partial (UV)}{\partial X} + \frac{\partial V^2}{\partial Y} = -\frac{\partial P}{\partial Y} + \frac{1}{Re}\left\{\frac{\partial^2 V}{\partial X^2} + \frac{\partial^2 V}{\partial Y^2}\right\} + \frac{Gr}{Re^2}.\theta \tag{3.2.3}$$

Energy :

$$\frac{\partial (U\theta)}{\partial X} + \frac{\partial (V\theta)}{\partial Y} = \frac{1}{Re.Pr}\left\{\frac{\partial^2 \theta}{\partial X^2} + \frac{\partial^2 \theta}{\partial Y^2}\right\} \tag{3.2.4}$$

where

$X = \frac{x}{L_{ref}}$, $Y = \frac{y}{L_{ref}}$, Reynolds number $(Re) = \frac{U_{ref}.L_{ref}}{\nu}$, $U = \frac{u}{U_{ref}}$, $V = \frac{v}{U_{ref}}$

Prandtl number $(Pr) = \frac{\nu}{\alpha}$, Grashof number $(Gr) = \frac{g\beta(T_h - T_c)L^3_{ref}}{\nu^2}$

and Richardson number $(Ri) = \frac{Gr}{Re^2}$

In case of isothermal problems, the energy equation (Eq. 3.2.4) need not be solved and the buoyancy terms in the V momentum equation (Eq. 3.2.3) is zero. For an isothermal lid driven cavity problem, the most obvious reference velocity is the lid velocity ($U_{ref} = U_L$) and the reference length is the length of the moving lid ($L_{ref} = L$). The same reference velocity can also be used for the mixed convection problem where the lid is driven. In that case the governing parameters are *Ri*, *Re* and *Pr*. For pure free convection problem where the flow velocities are induced by thermal effects only, an appropriate reference velocity is

a thermal velocity scale defined as α/L_{ref} where α is the thermal diffusivity. In that case the operating Reynolds number $Re = \alpha/\nu = 1/Pr$ or the inverse of the Prandtl number. Substituting Re as $1/Pr$ in Eqs. 3.2.2 to 3.2.4, one easily obtains the following non dimensional equations for pure free convection problem.

Continuity :

$$\frac{\partial U}{\partial X} + \frac{\partial V}{\partial Y} = 0 \tag{3.2.5}$$

U-Momentum :

$$\frac{\partial U^2}{\partial X} + \frac{\partial (UV)}{\partial Y} = -\frac{\partial P}{\partial X} + Pr\left\{\frac{\partial^2 U}{\partial X^2} + \frac{\partial^2 U}{\partial Y^2}\right\} \tag{3.2.6}$$

V-Momentum :

$$\frac{\partial (UV)}{\partial X} + \frac{\partial V^2}{\partial Y} = -\frac{\partial P}{\partial Y} + Pr\left\{\frac{\partial^2 V}{\partial X^2} + \frac{\partial^2 V}{\partial Y^2}\right\} + Ra.Pr.\theta \tag{3.2.7}$$

Energy :

$$\frac{\partial (U\theta)}{\partial X} + \frac{\partial (V\theta)}{\partial Y} = \left\{\frac{\partial^2 \theta}{\partial X^2} + \frac{\partial^2 \theta}{\partial Y^2}\right\} \tag{3.2.8}$$

where the controlling parameters are Rayleigh number ($Ra=Gr.Pr$) and the Prandtl number.

4 . NUMERICAL GRID FOR THE FLOW COMPUTATION

4.1 CARTESIAN GEOMETRY

4.1.1 Concept of subdomain grid

Two major tasks of any grid-generation algorithm are: (i) Geometric modeling for accurate numerical specification of the boundaries of a physical domain consisting of one or more arbitrary shaped configuration where the flow equations are to be solved and (ii) Generation of space grid *ie*., calculation of nodal coordinates of a structured grid network (a family of intersecting grid lines) covering the computation domain, using the specified point coordinates on the domain boundaries. However the task is quite simplified if cartesian grids are used when the mutually perpendicular grid lines are always parallel to the cartesian axes and therefore the task is simplified to specification of the nodal coordinates on the rectangular domain boundary only. Some of the problems might consist of salient boundary lines inside the computation domain separating some specific zones to be blanked as solid. In those cases it is appropriate to divide the whole domain into a number of sub-domains covering the different regions of interest. The concept is clarified later in subsection 4.1.3, where the application examples are presented.

4.1.2 Geometric Stretching

A systematic procedure is required to prescribe the coordinates of boundary nodes for any physical problem according to a desired intensity and location of stretching. On the physical space, each computational boundary may consist of one or more segments separated by salient points prescribed by the user. In a cartesian grid system the segments obviously are linear and the required grid nodes can be accurately prescribed on the boundary according to a pre-specified intensity and location of stretching.

The stretching functions used in the present work are purely one-dimensional *i.e*., the grid size increases or decreases only along the segment length, irrespective of whether the segment is straight or curved. Points are marked on a given segment in such a way that the grid size *ie*., the length between consecutive points, measured along the segment-arc (*L),* follows a geometric progression rule whose common ratio decides the extent of stretching. The points may be stretched either at the beginning or at the end or near the both ends of the segment, the number of grid points (*N)* to cover the segment including the ends, the common ratio(*R)* of the progression and a location index (*INDEX*) to indicate whether stretching is intended at the start or end or both ends of the segment. If *S* be the minimum grid size, measured along the segment-arc, the magnitude of *S* according to the geometric progression rule is:

$$S = \frac{L(R-1)}{(R^{N-1}-1)}$$

In case of stretching at both ends, the number of nodes must be odd and the arc is divided into two equal halves and each portion is stretched near the corresponding edge using

similar formulae. The grid generation routine for the present work has been developed at the CTFD division, NAL by Fatima *et al* (1994).

4.1.3 Cartesian Grid for the cavity

The computation domain here is very simple without any blanked region. The domain is taken as a unit square covered with 40 × 40 uniformly spaced grid. Fig. 4.1 shows the grid in unstretched form while Fig. 4.2 shows the grid in stretched form, where stretching is provided near the wall where steep gradients of the flow variables are to be accurately resolved.

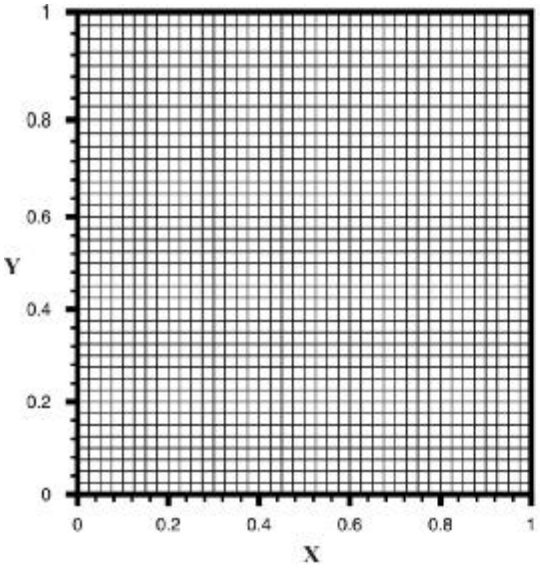

Fig 4.1 Uniformly spaced grid (40 ×40)

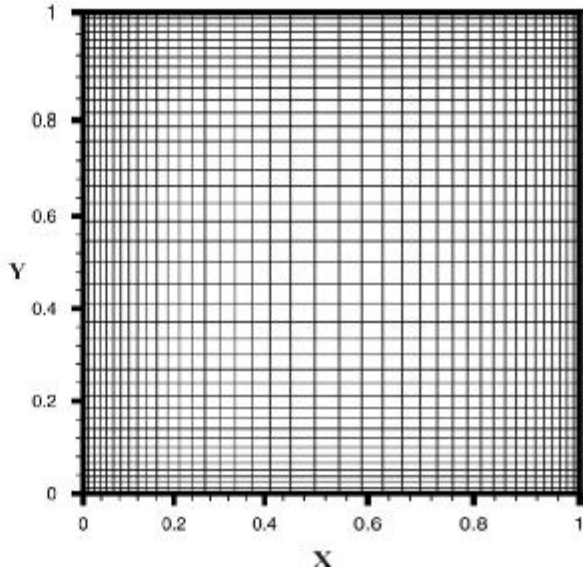

Fig 4.2 Stretched grid (40× 40 with Stretching ratio =1.12)

5. NUMERICAL SOLUTION OF FLOW EQUATIONS

5.1 FINITE VOLUME METHOD FOR SOLUTION OF FLOW EQUATION

The transport equation described in section 3 may be written in a generic form for the variable ϕ as :

$$\frac{\partial(U\phi)}{\partial x}+\frac{\partial(V\phi)}{\partial y}-\frac{\mu}{\Gamma_\phi}\left\{\frac{\partial^2\phi}{\partial x^2}+\frac{\partial^2\phi}{\partial y^2}\right\}=S_\phi \qquad (5.1)$$

5.1.1 Control volume and variable arrangement

In any finite volume method, the governing differential equations Eq. 5.1 for different dependent variables (ϕ) are to be integrated over a finite number of control volumes covering the computational domain formed by the grid generation procedure. Fig 5.1 shows the kind of control volume and the variable arrangement used in the present method. The grid generation procedure calculates the coordinates of the control volume vertices which are simply joined by linear segments to form the boundary plane and hence the volume. All the variables are stored at the geometric center *P* of the control volume. The four neighboring control volume centers are indicated by *N, S, E* and *W* for the north, south, east and west neighbors. The face center points *n, s, e* and *w* are located at the midpoint of the opposite edges. These points specified on edges are used for locating the variables and their gradients on the control volume faces. The cartesian velocities U_w & V_w *etc*., indicated in Fig. 5.1 for the west face of control volume are computed and finally the total convective mass fluxes at cell faces are stored.

5.1.2 Discretisation schemes for the flow equations

5.1.2.1 Flux balance equation

The difference equations representing the flux balance are derived by integrating the governing equations over the control volumes with the aid of the Gauss Theorem. Thus, the volume integral of the terms under the differential operator on the left hand side of the transport equation Eq. 5.1 may be converted to surface integrals (fluxes) over the four different faces of the control volume. The resulting balance equation for each control volume and variable ϕ may then be expressed as follows:

$$I_e - I_w + I_n - I_s = \int_{\Delta V} S_\phi dV \qquad (5.2)$$

where I_e, for example, represents the total flux of ϕ across the face ***e***. Each of the surface fluxes I_e, I_w *etc*. is made of two distinct parts, namely a convective contribution I^C, a

diffusive contribution I^D, which may be expressed for a typical cell face 'w' for the flow variable ϕ as

$$I_w^C = \rho \Delta y U_w \phi_w \tag{5.3.a}$$

$$I_w^D = \mu_w \frac{(\phi_W - \phi_P)}{\Delta x_{cw}} . \Delta y \tag{5.3.b}$$

The diffusive fluxes I_w^D at face 'w' is evaluated by linear interpolation between two cell centers (*P* and *W*) at either side of the face, whereas the convective flux is decided by the interpolation assumptions for evaluation of ϕ_w between the nodes *P* & *W*.

5.1.2.2 Convective flux discretisation

The numerical stability and accuracy of a RANS equation solver depends mainly on how the non-linear convective fluxes(I_w^C) are discretised. Three desirable properties for a good convective flux discretisation scheme are conservativeness, boundedness and transportiveness, which simultaneously ensure the stability and accuracy of the solution. The one-dimensional form of pure upwind scheme where the variable value at any cell face is replaced by the value at the immediate upstream node, satisfies all these three properties. But for multi-dimensional flows, where the flow is skewed to the grid system, the inaccuracies due to numerical diffusion contaminate the results to a considerable extent. The idea of combining the advantages of the stability and flow direction sensitivity of an upwind scheme and the high accuracy of a low-diffusion scheme even at high cell Reynolds number resulted in the development of a series of higher order upwind schemes which bring in the influence of more remote grid points through variable values or their derivatives. The so-called Central Difference scheme using linear inter-nodal variation is used for diffusive fluxes. But for high Reynolds number flow the central difference scheme is observed to create non-physical oscillations in the solution specially for coarse grids. A variety of low-diffusion high order Upwind schemes have therefore been formulated, assessed for their relative performance and used in the present algorithm. Three different schemes provided in the algorithm are Central Difference, Central/Upwind Hybrid [Patankar(1980)], and Quadratic Upwind scheme, QUICK [Leonard(1979)]. The detailed algebra of all these schemes are discussed elsewhere[Kulkarni *et al* (2001)].

All the calculations in the present work use the second order accurate central difference scheme .

5.1.3 Finite volume equation for momentum and energy

The convective and diffusive fluxes calculated according to the discretisation scheme used, when replaced in Eq. 5.2 lead to the conservation of fluxes in the form a linear equation for the respective flow variable solved. The source terms are often non-linear and in order to enhance the numerical stability, the source terms for the steady state equation are decomposed in to two components *SU* and *SP* in a linear form as following :

$$\int S_\phi dxdy = SU + \phi_p SP \tag{5.4}$$

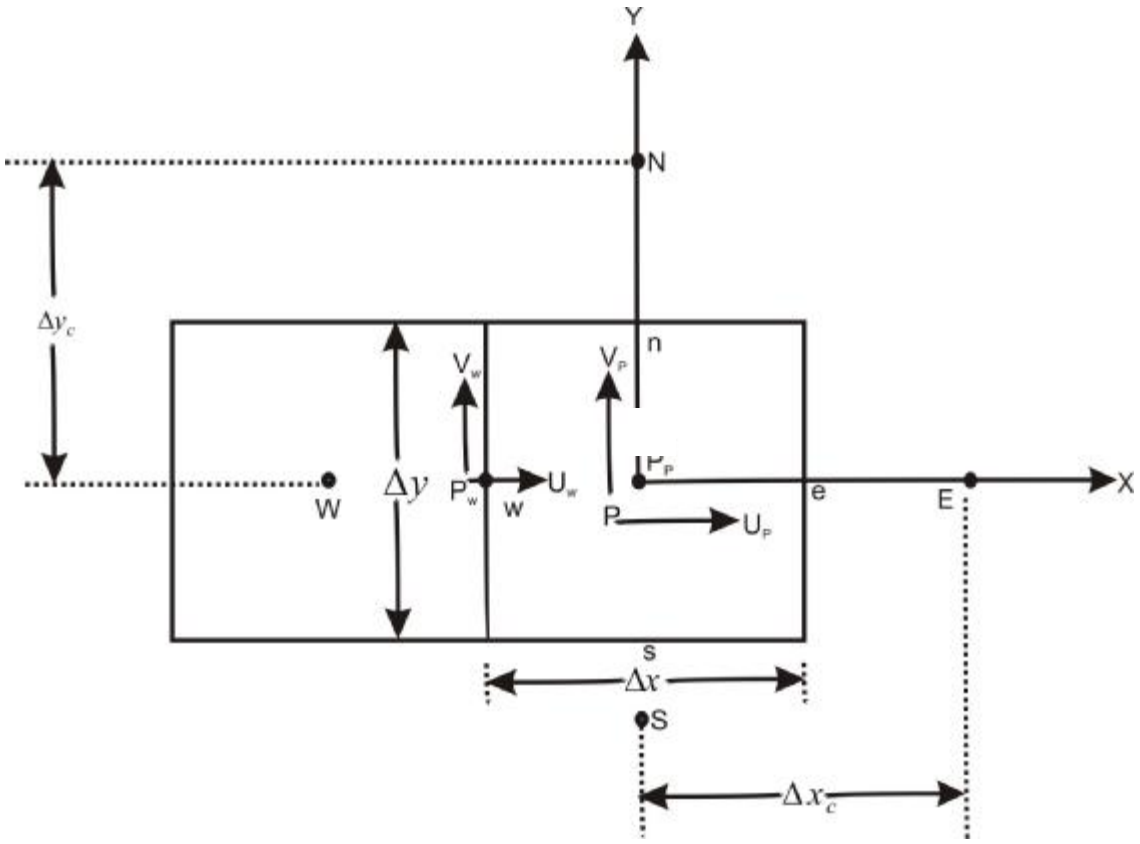

Fig. 5.1 Typical Cartesian Control Volumes

Replacing the different fluxes and the source terms, the flux balance equation Eq. 5.3 can be cast into the following quasi-linear form

$$\left(\sum A_i - SP\right)\phi_p^{n+1} = \sum_i A_i \phi_i^{n+1} + SU \tag{5.5}$$

where the coefficient $A_i's$ represent the combined effect of convection and diffusion across the cell face . However, transformation of the continuity equation to an equation of pressure correction, is not that straightforward and is described in the following section.

5.1.4 Calculation of pressure field

The present algorithm calculates the pressure field using the SIMPLE algorithm of Patankar *et al* (1972), modified for a co-located variable arrangement. The basic idea of the SIMPLE algorithm is (i) to assume an artificial link between the cell-centered pressure and the cell-face velocities from the discretised momentum equations, (ii) to frame a system of linear equations for pressure correction that satisfy continuity and (iii) finally to correct the pressure and velocities accordingly. For two-dimensional flows, the discretised momentum equations express the cell-centered velocities as**:**

$$U_P = \alpha_v \left[H_u + D_u \left(P_w - P_e \right) \right] + \left(1 - \alpha_v \right) U_p^0$$
$$V_P = \alpha_v \left[H_v + D_v \left(P_s - P_n \right) \right] + \left(1 - \alpha_v \right) V_p^0$$

$$\text{where , } \quad H_u = \frac{\left(\sum A_{nb} U_{nb} + SU \right)}{A_P^u} \quad ; \quad H_v = \frac{\left(\sum A_{nb} V_{nb} + SU \right)}{A_P^v} \qquad (5.6)$$

$$\text{and} \quad D_u = \frac{\Delta y}{A_P^u} \quad ; \quad D_v = \frac{\Delta x}{A_P^v}$$

A_{nb} represents the coefficients for neighboring nodes, the superscript '0' is the value at the previous iteration and A_P^u and A_P^v are the value of A_P for U & V at the node P and α_v is an under-relaxation parameter. According to the *Momentum Interpolation Scheme* [Majumdar (1988)], the typical cell-face velocity at the west face may be expressed as:

$$U_w = \alpha_v \left[\overline{H_u} + \overline{D_u} \left(P_W - P_P \right) \right] + \left(1 - \alpha_v \right) U_w^{\,o}$$
$$V_w = \alpha_v \left[\overline{H_v} + \overline{D_v} \left(P_S - P_P \right) \right] + \left(1 - \alpha_v \right) V_w^{\,o} \qquad (5.7)$$

where the expressions with overbar represent the linear average of the same quantities evaluated at the cell-centers P and W adjacent to the face `w'. Now the velocity components U_w & V_w satisfying the momentum equations do not necessarily satisfy the following equation for cellwise continuity

$$C_e - C_w + C_n - C_s = 0 \qquad (5.8)$$

In order to satisfy continuity, the velocity field needs to be corrected and the convective mass-flux C_w for the west face, for example, may be written as:

$$C_w = \rho_w \Delta y (U_w + U_w^{'}) \qquad (5.9)$$

using the perturbation form of eqs. 5.6 & 5.7,the relationship between pressure correction and velocity correction for cell centre *p* and cell face '*w*' may be expressed as :

At the cell center :

$$U'_p = \alpha_v D_u \left(P'_w - P'_e\right) \quad \text{and} \quad V'_p = \alpha_v D_v \left(P'_s - P'_n\right) \tag{5.10}$$

and

At the cell face :

$$U'_w = \alpha_v D_u \left(P'_W - P'_P\right) \quad \text{and} \quad V'_w = \alpha_v D_v \left(P'_S - P'_P\right) \tag{5.11}$$

Substitution of the cell-face velocities U_w *etc.,* from equations similar to Eq. 5.7 and the corrections U'_w *etc*., from equations similar to Eq. 5.11, leads to a system of linear equations for P', expressible in the form of the general equation Eq. 5.5. Cell center pressures (P_P) are then corrected by an amount $\alpha_P P'$ where α_P is an underrelaxation parameter and corrections are applied to the two cell-centered velocity components according to Eq. 5.10 and to all the cell-face velocity components on the four cell faces according to correction equation similar to Eq. 5.11.

5.1.5 Sequence of the solution algorithm

The sequence in which the calculation is carried out is as follows:

1. Set initial field values of flow variables ($U, V, P \& \theta$).
2. Solve the momentum equations to obtain U and V field.
3. Compute cell-face velocities(U_w, V_w etc) using Momentum Interpolation between adjacent control volumes; compute cell-wise mass imbalance and solve for the pressure correction (P') field.
4. Correct the pressure field and velocities at cell center and cell faces.
5. Solve the energy equation to obtain the temperature (θ) field.

Repeat steps (2) to (5) with updated pressure ,velocities & temperature field till convergence between two consecutive time steps.

5.1.6 Convergence Criteria

5.1.6.1 General Convergence Criterion

Convergence is declared when the maximum normalized sum of the absolute residual sources over all computational nodes is less than a prescribed limit, the so-called convergence criterion. The normalized L_2 norm of the residual for the variable ϕ after n iterations may be calculated as:

$$R_\phi^n = \sqrt{\sum_N \left(\sum_{nb} A_{nb}\phi_{nb} + SU - A_p\phi_p^{n-1} \right)^2} \; / RNORM_\phi \tag{5.12}$$

where N = total number of computational nodes, $RNORM_\phi$ = a reference quantity used for normalization, $\sum_N$ is the summation over all the control volumes and $\sum_{nb}$ is the summation over all neighbouring nodes for each control volume. The maximum value of R_ϕ^n from all ϕ solved is checked against a specified convergence criterion in order to stop the computation cycle. The value of convergence criterion used for most of the examples presented is 10^{-5}. As stated earlier, sufficient inner iterations are however carried out for the pressure correction in order to satisfy continuity to a considerable extent after every outer iteration loop. The pressure correction sweep for each outer iteration cycle is terminated when either number of sweeps exceeds 10 or the residual is reduced to 10 % of its starting value.

5.1.6.2 Special convergence criteria for heat transfer problem

It has been observed in some of the computations that using the maximum normalised residual of the mass, momentum and energy equations as stopping criterion for the iterative solution procedure, may often lead to a prohibitive computation time requirement. Most of the time when the flow pattern is almost stabilised, the numerical process does not bring any significant change in the flow field but the residual may still be somewhat high due to one or two singular nodes with incompatible boundary conditions. In order to avoid such uneconomic computation, some special convergence criterion suggested by Moallemi *et al* (1992) has been attempted in the present work. For any set of input parameters, the solution is considered converged if

$$\left|\phi^{k+1}(i,j) - \phi^{k}(i,j)\right| \Big/ Max\left|\phi^{k+1}(i,j)\right| < 10^{-3} \quad \text{and} \quad \left|1 - \left(Nu_c / Nu_H\right)\right| < 10^{-3}$$

Where I and j refer to the computational node index, k is the iteration loop counter, ϕ is U, V or θ and Nu_H and Nu_C are area –averaged Nusselt numbers on the lid and the bottom surfaces, respectively. It has been observed that when the above criterion is satisfied, the normalised continuity residue is also below the acceptable limit of 10^{-6}. Usually 2000 to 2500 iterations are required depending on the input parameters.

6. RESULTS AND DISCUSSION

6.1 ISOTHERMAL LID-DRIVEN SQUARE CAVITY

This problem is chosen to understand the different features of the existing implicit finite volume type Navier Stokes code RANS2D and to validate the same against the available bench-mark results of Ghia & Ghia (1982). Development of laminar flow in a lid-driven cavity is a work-horse kind of test problem often used for validation of any new CFD code/algorithm. The flow being confined from all four sides is an example of a recirculating flow induced by the moving wall forming the top lid of a square shaped box with the other three walls at rest. Although the geometrical and physical boundary conditions are simple and unambiguous, the physics of such strongly recirculating flow however is quite complex. The flow computations are carried out for Reynolds number Re=100 & Re=1000 based on lid velocity and the effect of convergence criteria ,grid resolution and convective flux scheme on the flow solution have been studied in details.

6.1.1 Computational Details

The computation domain in the form of a unit square is usually covered by equally spaced nodes along both the directions and a typical grid of 101×101 is shown in Fig. 6.1(a). The number of grid nodes, however are varied in order to study the effect of grid size on the flow pattern. The flow boundary conditions are shown in Fig 6.1(b)

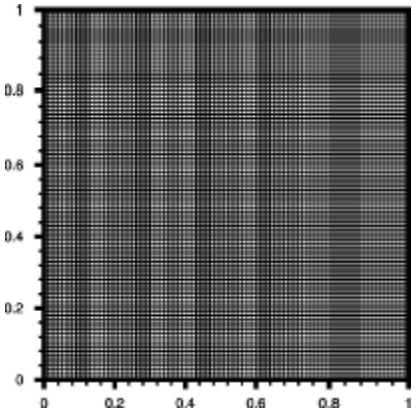

(a) Grid : 101×101

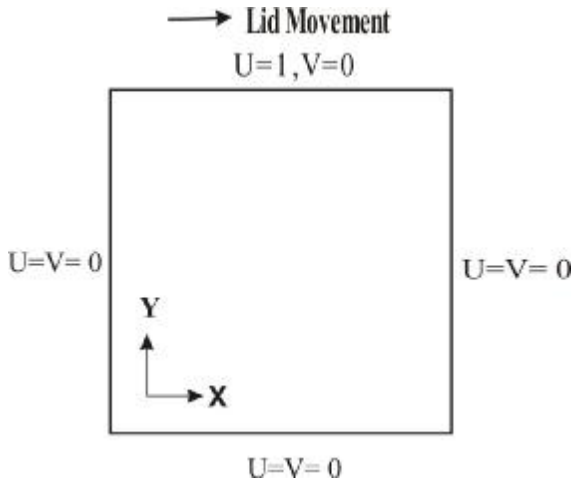

(b) Boundary conditions

Fig 6.1 Numerical grid and boundary conditions for single block flow computation

6.1.2 Effect of Convergence Criterion

The usual convergence criteria of checking the maximum normalized L2 –norm of the residue of each equation is described in Section 5. Numerical experiments have been carried out to examine the effect of convergence criteria on the accuracy of the solution obtained when three values of the criterion ε *viz.,* 10^{-4}, 10^{-5} and 10^{-6} are chosen. The predictve-corrective procedure of SIMPLE (Semi-Implicit Method for Pressure Linked Equation) Algorithm (Patankar(1980)) is used with α_p=0.2, α_u=α_v=0.8 where α_p, α_u and α_v are the under-relaxation factors for pressure, u-velocity and v-velocity respectively. Fig. 6.2(a) shows the U-velocity profile at X=0.5 and Fig. 6.2(b) shows the V-velocity profile at Y=0.5, computed with different convergence criteria and compared to the benchmark computation of Ghia *et al* (1982). This figure clearly indicates insignificant difference between the results obtained using $\varepsilon = 10^{-5}$ and $\varepsilon = 10^{-6}$. One therefore needs to solve the equations at least up to a convergence level of 10^{-5} to obtain sufficiently accurate results. All computations for the thermal cavity problem have been carried out using $\varepsilon = 10^{-5}$.

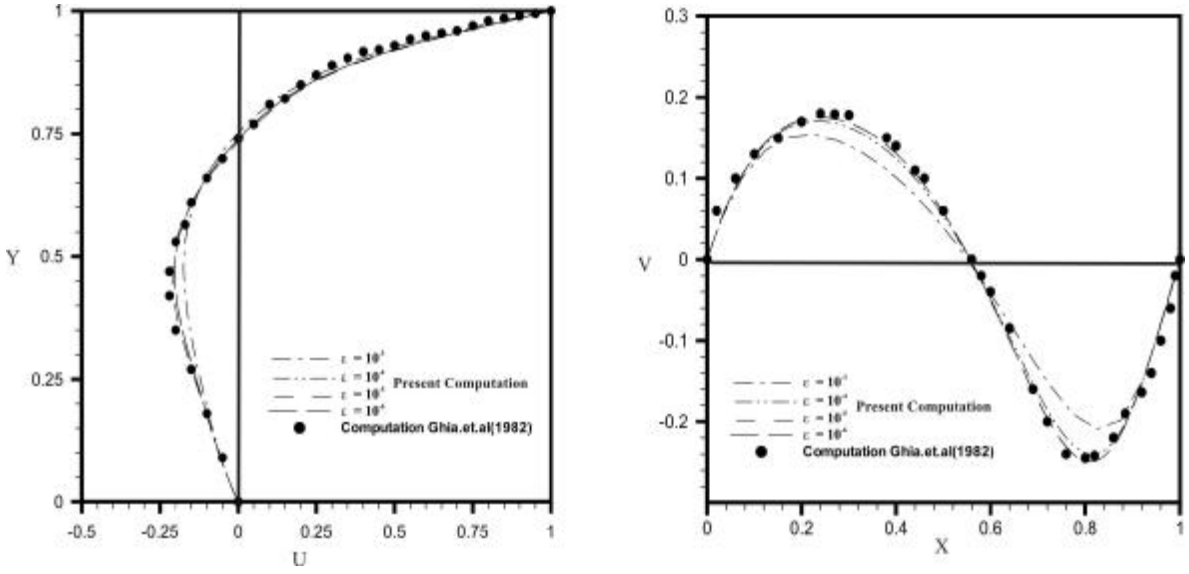

(a) Transverse distribution of longitudinal velocity at X=0.5

(b) Longitudinal distribution of transverse velocity at Y=0.5

Fig 6.2 Comparison of velocity profiles obtained using different convergence criteria for lid driven cavity flow (Re = 100)

6.1.3 Effect of Grid Resolution

Four different equi-spaced grid sizes 21×21, 41×41, 81×81 and 101×101 are used to check the sensitivity of the grid resolution on the flow results computed with different grid sizes and the central difference scheme for the convective flux discretisation.

In Fig 6.3 shows the U & V -velocity profile at X=0.5 and Y=0.5 respectively computed with four different grid sizes. The figure indicates clearly that beyond a grid size of 81×81, more or less grid independent results are obtained. 81×81 grid has therefore been used in all further computations of the present thermal cavity problem both in case of free convection and mixed convection cases.

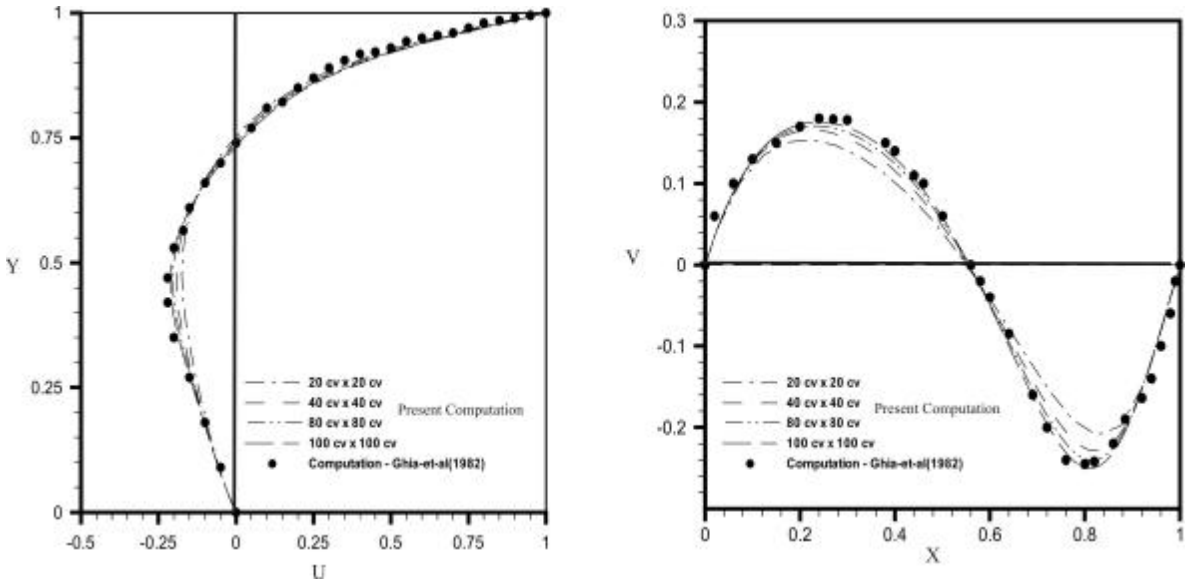

(a) Transverse distribution of longitudinal velocity at X=0.5

(b) Longitudinal distribution of transverse velocity at Y=0.5

Fig 6.3 Effect of grid resolution on computation results

6.1.4 Effect of Convective Discretisation Schemes

Four different spatial discretization schemes *viz.,* Central Difference , pure Upwind, Hybrid and QUICK schemes are used employing the 81 × 81 grid. Fig. 6.4 shows the effect of the discretization scheme on the velocity profiles U and V at X=0.5 and Y=0.5 respectively. The figure clearly reveals that using a reasonably fine grid, the first order accurate pure upwind scheme is under-predicting the velocity filed due to its usual numerical diffusion problem for multidirectional flow. On the other hand, no significant difference is observed between the benchmark solution and the solutions obtained from different high order schemes: specially the results of the QUICK and HLPA schemes are observed to be almost coinciding. In the present work on laminar flow and heat transfer in a lid driven square cavity, second order accurate central difference scheme has consistently been used for the momentum equations in all the problems considered.

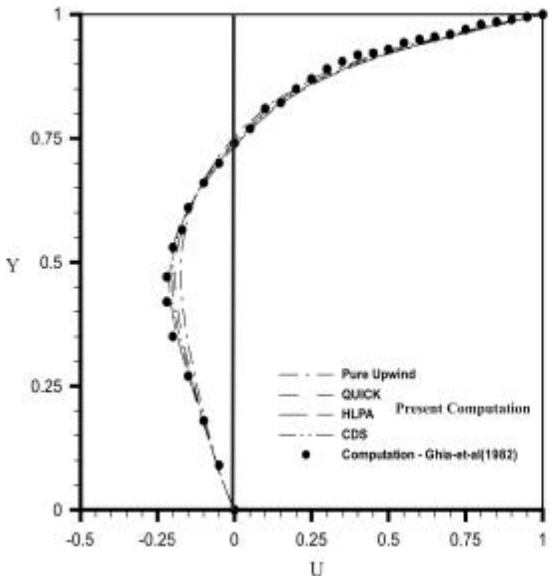

(a) Transverse distribution of longitudinal velocity at X=0.5

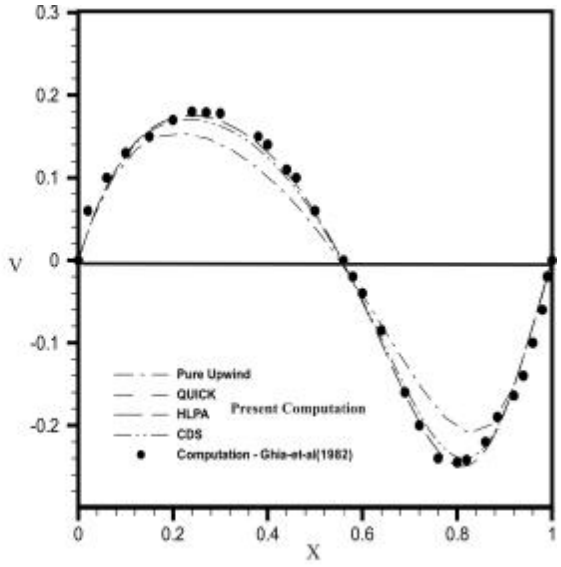

(b) Longitudinal distribution of transverse velocity at Y=0.5

Fig 6.4 Effect of convective flux scheme on computation results

6.1.5 Streamline and Velocity field

Fig. 6.5 shows the particle traces (streamlines for steady flow) computed using 81 × 81 grid and the central difference scheme for convective flux discretisation for two different flow Reynolds numbers (*Re*=100 and 1000), based on the lid velocity. The computed streamlines clearly show the prediction to be physically realistic with the formation of a large primary vortex covering most of the cavity space and a couple of small secondary vortices at the left bottom and the right bottom corner of the cavity. The location of the centers of the primary and the two secondary vortices are found to be in close agreement with the computation reported by other researchers in the available literature

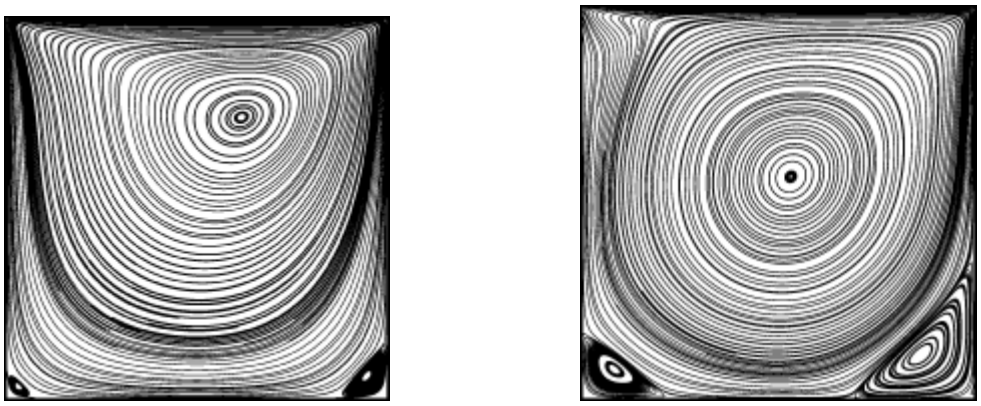

(a) Streamlines at Re=100 **(b) Streamlines at Re=1000**

Fig 6.5 Streamlines obtained using single block computations for flow in a lid driven square cavity

Primary recirculating eddy is generated by the lid dragging the adjacent fluid. The vortex is clockwise when the lid is dragged from left to right. Both the counterclockwise secondary eddies are formed near the corners due to the separation of the boundary layer growing along the corresponding wall , under the adverse pressure gradient caused by the stagnation effect of another wall at right angle. As the Reynolds number is increased to 1000 , the primary vortex moves towards the cavity centre and the size of the secondary eddies is larger than those for *Re*=100.

6.2 LAMINAR NATURAL CONVECTION IN A BOTTOM HEATED CAVITY

This test case is chosen to check whether the flow physics can be properly captured by the flow solution algorithm when the cavity has an aspect ratio other than unity and it is heated from the bottom with the side walls thermally insulated. In this case the reference length and reference velocity are chosen as H and α / H respectively for non-dimensionalisation of the governing equations. It is observed experimentally that when a horizontal viscous fluid layer is heated from below, the imposed temperature difference must exceed a finite critical value before the first signs of fluid motion and convective heat transfer are detected. The condition for onset of convection in a rectangular cavity is often expressed by a critical Rayleigh number where $Ra = g\beta(T_h - T_c)H^3 / \nu\alpha$. In this case , the acceleration due to gravity (g) acts along the vertical downward direction, H is height of the cavity with top wall maintained at a lower temperature T_c and the hot bottom wall is maintained at T_h. As long as the temperature difference ($T_h - T_c$) is below certain threshold , heat is transferred in the conduction mode only without any fluid motion. Beyond a critical temperature difference, the static conduction state becomes unstable to any small disturbance and the transition takes place from the conduction to convection mode of heat transfer. The Rayleigh number corresponding to this critical temperature difference is called the critical Rayleigh number. Another interesting phenomenon observed in experiments is the

formation of multiple vortical cells in the flow along the longer side of the cavity when heated from the bottom wall.

6.2.1 Computational Details

In the present calculations for cavity with bottom heating, three different aspect ratios, *viz.*, H/L = 0.5, 1.0 and 2.0 are considered where H represents the distance between the horizontal isothermal walls and L represents the distance between the vertical adiabatic walls. The schematic arrangement of the cavity with the flow boundary conditions used for the computation are shown in Fig. 6.6

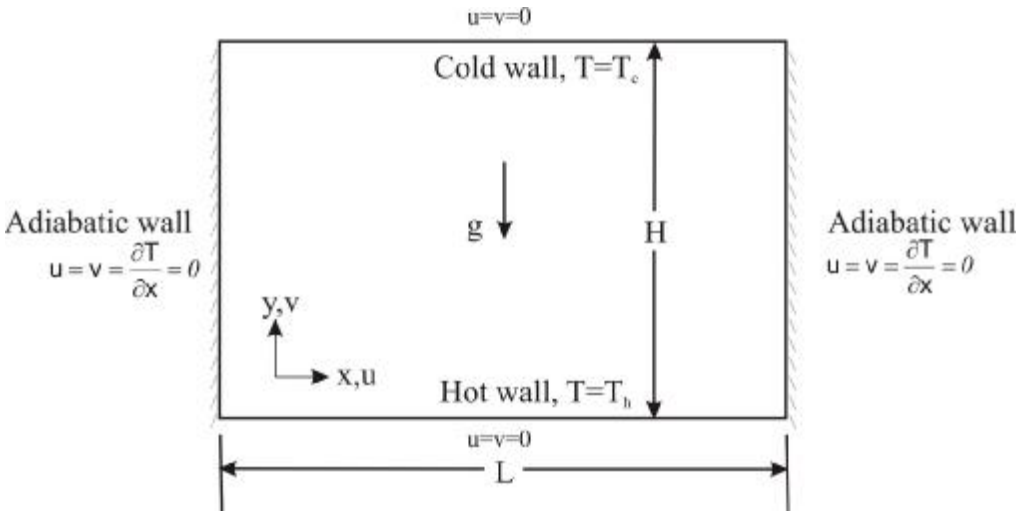

Fig 6.6 Boundary condition for stationary rectangular cavity with bottom heating

6.2.2 Variation of Nusselt number with Rayleigh number

In order to determine the critical value of *Ra,* computations are first carried out with a 81×41 grid for an aspect ratio of 0.5, for the values of *Ra* ranging from 1000 up to *Ra*= 1700, the $\overline{Nu}$ is found to be 1 and beyond this value of *Ra* only the $\overline{Nu}$ increases with *Ra*. Recomputation of the flow field between *Ra* = 1700 and *Ra* =1800 in steps of 10 indicates the critical *Ra* at 1710 against a theoretical value of $\overline{Nu}$ =1707.76 reported by Xu *et al* (1998). Finally Fig. 6.7 shows the variation of average Nusselt number as the *Ra* is changed from 1000 to 100,000 and the results are compared to the computation results reported by Clever & Busse (1974) . Reasonable agreement is observed between the two different computation results**.**

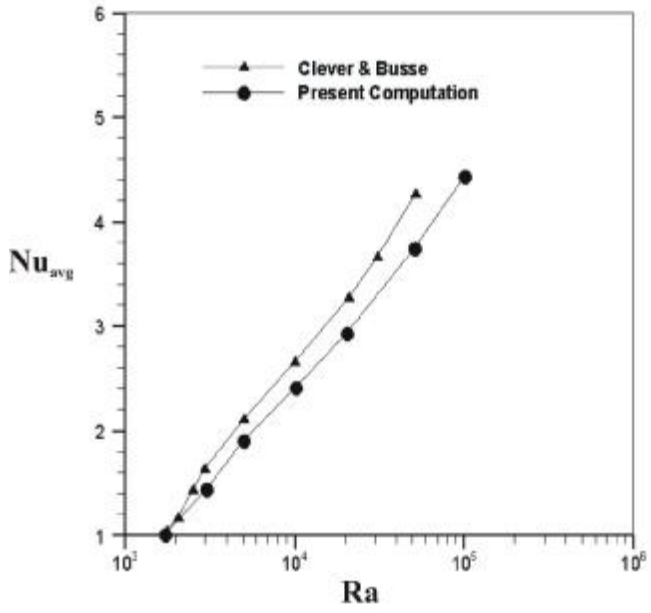

Fig 6.7 Variation of Average Nusselt number with Rayleigh number for bottom heated cavity with H/L=0.5

6.2.3 Streamline and Temperature Field

Fig. 6.8(a) shows the streamline pattern for three different aspect ratios 0.5, 1.0 and 2.0 at $Ra = 10^4$. When the aspect ratio is 0.5 , the computation shows the formation of two vortical structures along the longer side of the cavity which are usually designated as the Rayleigh- Bernard convection cells. Close to the left vertical wall, a counter-clockwise vortex is formed whereas the other vortex near the right wall rotates in a clockwise sense. The corresponding isotherms shown in Fig. 6.8(b), indicates a symmetry about the vertical axis passing through the middle of the cavity. On the bottom plate the thermal boundary layers appear to be somewhat thinner towards the side walls and a large portion of the heat conducted near the outer part of the bottom plate is transported by convection through the central region. However for aspect ratio 1.0, only one convective cell is formed occupying the central part of the cavity and two very small vortices are formed - one near the upper left corner and another near the right- bottom corner of the cavity. The corresponding isotherms show the relatively strong vertical temperature gradient near the left top and right bottom corner of the cavity. The vortex core is maintained at a relatively low temperature with mild gradient along the horizontal direction whereas the heat conducted in the boundary layer of the bottom plate is transported by the vortical convection current and consequently conducted once again to the top colder wall in the boundary layer region. For an aspect ratio of 2.0 when the vertical side is taller, two convective cell structures are observed once again along the longer side, as in the case of aspect ratio of 0.5. The

isotherms also indicate a symmetry about the horizontal plane passing through the midheight of the cavity. Since the Rayleigh number based on the cavity height is maintained at the same value for the three cases, the effective temperature difference driving the flow varies from a large value at low aspect ratio to a relatively smaller value for a large aspect ratio case. This difference in temperature gradient in the three cases is clearly observed in the isotherms shown in Fig. 6.8 (b) where the crowding of the isotherms near the top and the bottom wall indicates the temperature gradient to be the sharpest in case of aspect ratio of 0.5 which eventually gets milder as the aspect ratio increases. Computation at three different aspect ratio shows that a proportionate increase in distance between the isothermal walls is likely to produce an equivalent number of convective cell structures in the cavity. The present trend of formation of multiple convection cells and the corresponding isotherms computed for aspect ratio other than unity compare reasonably well with the computation of Xu *et al* (1998) for aspect ratio of 0.5 and the results of flow visualization experiments reported by Mohamad *et al* (1993) for an aspect ratio of 0.1.

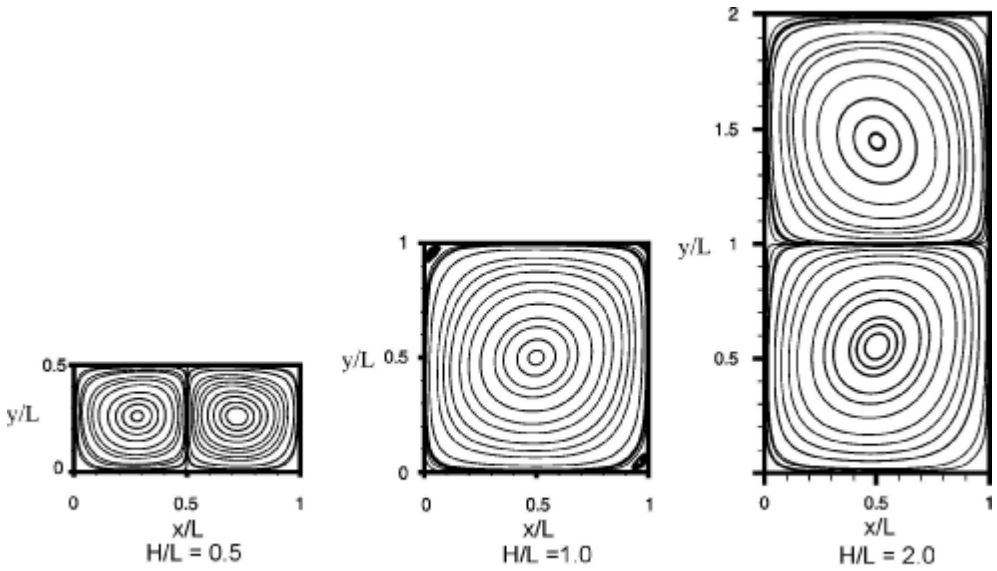

(a) Predicted streamlines from present computation

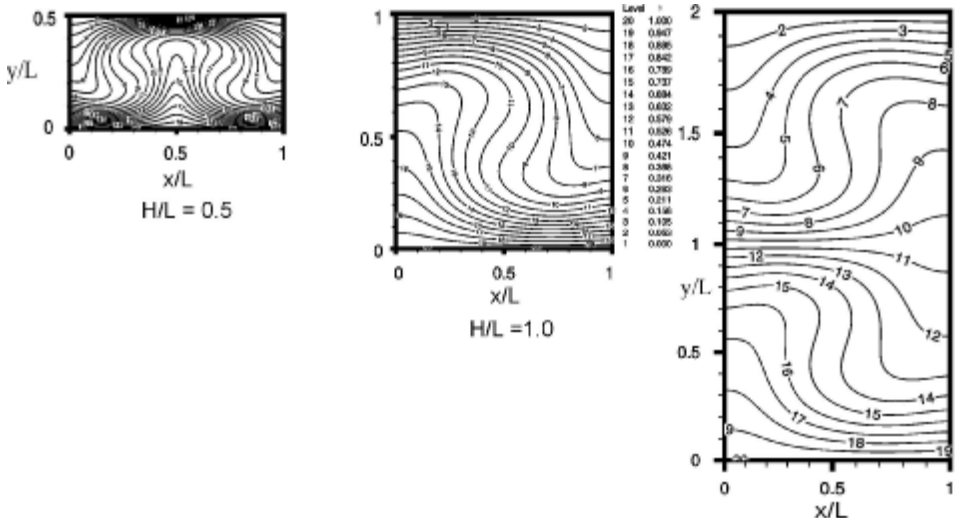

(b) Predicted isotherms from present computation

Fig 6.8 Effect of aspect ratio on flow and temperature field in a bottom heated stationary cavity (H/L=0.5,1,2.0) for Ra=10^4 ,Pr=0.71

6.3 LAMINAR FLOW AND HEAT TRANSFER IN A BOTTOM HEATED LID- DRIVEN SQUARE CAVITY

This section discusses the results on the mixed convection problem in a bottom heated square cavity which forms the main objective of the present work. The top lid of the cavity is moved from left to right with a uniform velocity U_L which eventually drives the cavity fluid due to the shear effect created at the top. This external boundary movement of the cavity is responsible for the forced convective heat transfer inside the cavity. Further, the cavity bottom is kept at a higher temperature relative to that at the top and the temperature difference causes the buoyancy effect which tends to create the upward movement of the fluid against the downward gravitational pull. Thus the flow pattern and the heat transfer inside the cavity is decided by a complex interaction between the shear and the buoyancy forces. The governing equations in non-dimensional form , discussed in Section 3, have already indicated that for mixed convection in a square cavity, the dimensionless physical parameters which decide the flow pattern and heat transfer are Reynolds number *Re*, Richardson number *Ri* and the fluid Prandtl number *Pr*. A parametric study has therefore been conducted to study the effect of different parameters on the flow pattern and the local and average heat transfer rates.

6.3.1 Computational Details

A uniform grid of size 81× 81 and a second order accurate central difference scheme has been used for the convective flux discretisation for all the computations carried out for the parametric study of the mixed convection problem in a square cavity. Computations are carried out for four different values of Richardson number (Ri = 0.01, 0.1,1.0 and 10) and three different values of Prandtl number (Pr = 0.1,1 and 10). The lid velocity based Reynolds number for all the cases is kept unaltered at Re = 1000 and the value of Ri is varied by changing the corresponding value of the Grashof number.

6.3.2 Effect of Prandtl number on the flow and heat transfer

Figs. 6.9-6.11 show the effect of Prandtl number on the flow and temperature fields in the cavity operating at three different values of *Ri*., decided by the specified lid velocity (shear) and the prescribed temperature difference (buoyancy) between the bottom and the top walls of the cavity respectively. Fig. 6.9 shows the Prandtl number effect at a relatively low value of the Richardson number ($Ri = Gr/Re^2$ =0.01 when Re=1000 and Gr=10^4). The flow fields for all the Prandtl numbers are found to be established due to the shear induced by the moving lid. This may be confirmed by the isothermal situation for the lid driven cavity problem at the same Reynolds number. The fluid flow is essentially characterized by (1) a primary recirculating eddy covering most of the cavity space, (2) a secondary eddy, often referred in the literature as the Downstream Secondary Eddy (DSE), formed at the right bottom corner between the vertical wall and the hot bottom surface as a result of flow separation on the right vertical wall due to the adverse pressure gradient near the corner stagnation region and (3) another secondary eddy referred as Upstream Secondary Eddy (USE) formed at the left bottom corner of the cavity as a result of flow separation on the bottom wall. All these features of flow are present even in absence of the buoyancy,

irrespective of the three values of *Pr* investigated. Moreover the size, position and strength of the secondary eddies are almost identical for the three cases presented. It is therefore confirmed that at low values of *Ri* (*Ri* =0.01 in Fig. 6.9 and *Ri*=0.1 in Fig.6.10) , the flow in the cavity is dominated by the shear action of the moving lid only. The flow represented by the streamlines is almost independent of the Prandtl number which, in principle, decides the temperature and buoyancy variations in the cavity. The corresponding variation of temperature field demonstrates strong dependence on the value of *Pr*. The thermal boundary layers thicken as the Prandtl number is reduced from 10 to 0.1 and the large constant temperature core which extends to most of the cavity space for *Pr*=10, gradually disappears as *Pr* is decreased to 0.1 or less. Since the core is nearly isothermal for large values of *Pr*, the influence of buoyancy is limited to the boundary layers only and it is manifested in the reduction in size and strength of the secondary vortices only (disappearance of the upstream secondary eddy for *Pr* =10 in Figs. 6.9 and 6.10) with increasing values of *Pr*. However, the strong dependence of temperature distribution on *Pr* is not significantly reflected on the flow pattern in the cavity for *Ri*=0.01 and *Ri*=0.1, which again shows the insignificant contribution of buoyancy in the flow development for *Ri* less than unity. Such observations have been reported earlier by Moallemi *et al* (1992) in their computation and also in the measurement of Prasad *et al* (1996). The flow pattern however undergoes some drastic change in Fig. 6.11 where the Grashof number is maintained at 10^6 and the Reynolds number is kept at 1000 which makes the Richardson number *Ri* to be unity. At this value of *Ri*, a strong effect of Prandtl number is observed on both the flow pattern and the temperature field. The fluid flow in the cavity seems to be established by a balance between the two driving mechanisms involved – the shear and the buoyancy effects. For a low value of *Pr* =0.1 , the heat transfer is mostly by conduction resulting in a rather gradual variation of temperature in the cavity, and therefore a relatively weak buoyancy field. The strong shear effect produces the primary vortex core as well as the three different secondary eddies including one near the top left corner which usually is formed in isothermal situation for *Re* greater than 1000 only. At *Pr*=1.0 , the balance between the shear and the buoyancy effects is manifested in the formation of two eddies of almost equal size. The upper one is driven by the moving lid and this is the primary vortex enclosing an approximately constant temperature core, with sharp temperature gradient near the top cold wall. On the other hand the bottom eddy is basically the enlarged form of the DSE near the right bottom corner, observed at lower values of *Pr*. As the Prandtl number increases further to 10, the heat transfer is mostly by convection in the boundary layers, the core of the cavity remains almost isothermal and the buoyancy effects are significant only near the walls, leading to an increased size of the DSE and elimination of the USE.

6.3.3 Effect of Richardson number on the flow and heat transfer

The effect of Richardson number (*Ri*) on the flow and temperature field at *Pr*=1 and *Re*=1000 for mixed convection in a bottom heated square cavity, is shown in Fig 6.12. At low values of *Ri* (no buoyancy in Fig 6.12 (a) and very mild buoyancy in Fig 6.12 (b), the effect of shear is dominant relative to the buoyancy effect. A large primary eddy with small upstream and downstream secondary eddies and a constant temperature core is observed

with large temperature gradient in the near wall thermal boundary layer only. When *Ri* is changed from 0 to 0.1, the only effect of buoyancy is manifested through the change of location and size of the secondary eddies (USE is reduced and the DSE size is increased to some extent). At *Ri*=1, the formation of two eddies of almost equal size, demonstrates the balance between shear and buoyancy effects. The upper primary eddy driven by the moving lid is deformed due to the opposing action of buoyancy on the right wall. In the bottom half of the cavity, the downstream corner eddy assisted by the upward buoyancy effect near the vertical downstream wall grows in size and covers almost half of the cavity. When *Ri* is increased to 10, the large buoyancy effects are confined to the thin thermal boundary layers only and a single primary vortex core with an approximately constant temperature is formed once again.

6.3.4 Variation of local Nusselt number along the hot wall

The variation of local Nusselt number along the hot bottom and the cold top wall of the cavity for different values of *Ri* and *Pr* is shown in Fig 6.13. Along the top cold lid surface the local Nusselt number always drops in the direction of the lid motion due to the growth of the hydrodynamic as well as the thermal boundary layer along this surface. But on the hot surface however the variation of local heat transfer rate is quite complex and this exhibits local maxima and minima which are decided by the location and strength of the primary and secondary eddies on this surface. The local *Nu* on the hot plate shows a maxima in the vicinity of the point where the cold jet from the top impinges the cavity floor. The drop in the local *Nu* from its peak value may be attributed to the formation and growth of the boundary layer along the cavity floor after the impingement. The points of the relative minimum correspond to the points of detachment of the boundary layers from the cavity floor due to flow separation. For $Ri < 1$ shown in Fig. 6.13 (a) and (b), the local peak and the averaged heat transfer rates over the lid as well as the hot bottom wall of the cavity increase with increase of *Pr*. This consistent trend is manifested over both the surfaces since the curves do not intersect at any location. The heat transfer in the cavity in these cases is dominated by the shear flow which dictates the primary recirculation in the cavity. The effect of buoyancy on the local heat transfer rate from the cavity floor is minimal since the position of maximum and minimum *Nu* do not change with a change of *Pr*. The minor change of local variation of *Nu* with *Pr* is due to the weak influence of the buoyancy of the secondary eddies. In Fig. 6.13 (c) when $Ri = 1$, the variation of Nusselt number along both hot and the cold wall illustrates stronger dependence on Prandtl number *Pr,* indicating significant contribution of buoyancy to heat transfer and fluid flow in the cavity. The points of maxima and minima correspond to the impingement on the cavity floor and separation from the floor respectively. The values of the Nusselt number increase in magnitude with the increase of Prandtl number for both the walls and considerable change is also observed for the location of the maxima for the *Nu* on the hot plate with the increase of the Prandtl number. This observation confirms that for *Ri* greater than or equal to 1, the buoyancy effects are sensed by both the primary and secondary eddies specially when *Pr* is greater than 1.

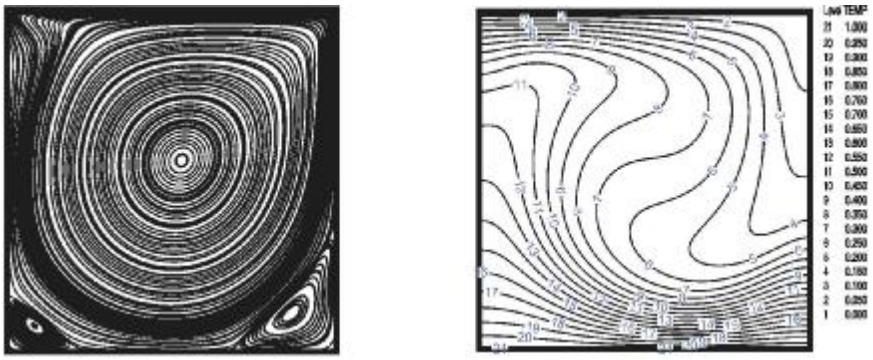

Pr = 0.1

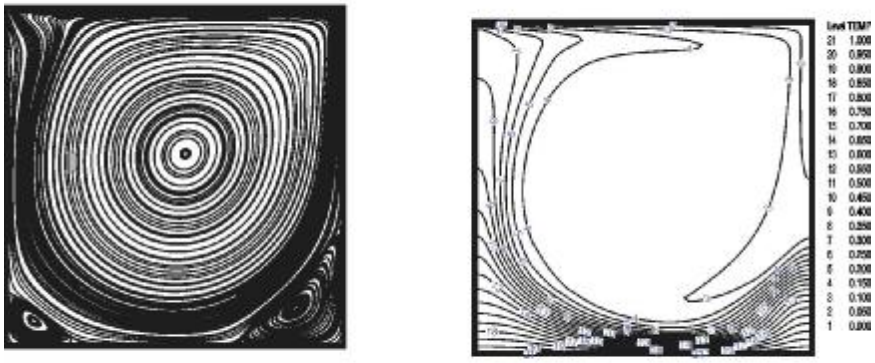

Pr = 1.0

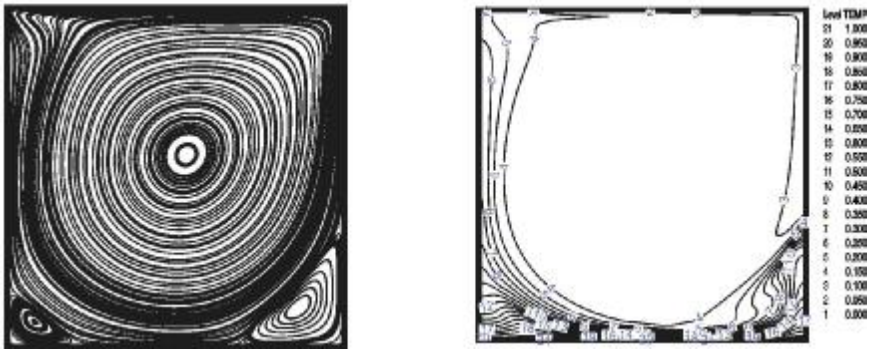

Pr=10.0

Streamlines **Isotherms**

Fig 6.9 Flow and temperature field in a cavity due to mixed convection for Re=1000 & Gr=10^4 (Ri=0.01)

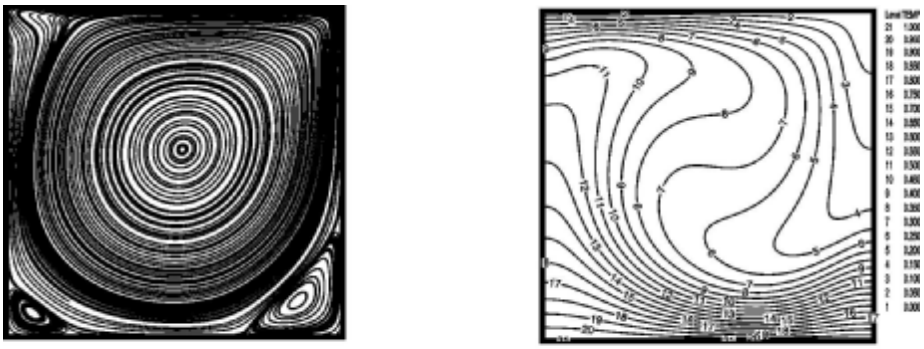

Pr = 0.1

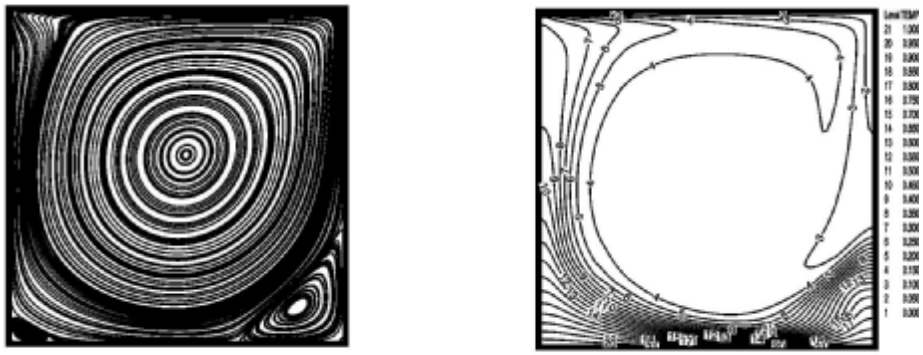

Pr = 1.0

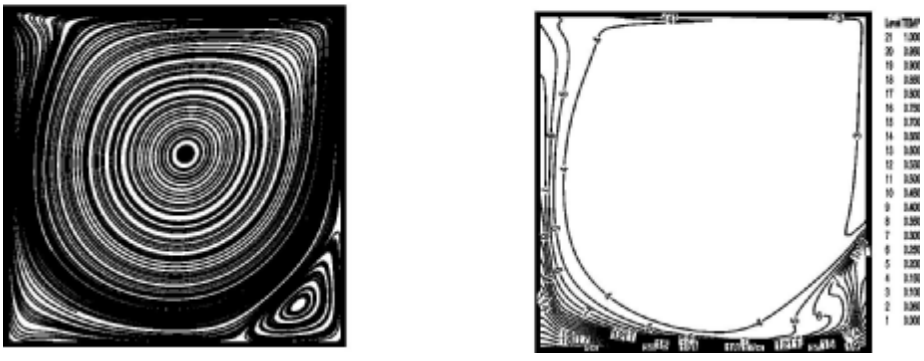

Pr=10.0

Streamlines **Isotherms**

Fig 6.10 Flow and temperature field in a cavity due to mixed convection for Re=1000 & Gr=10^5 (Ri=0.1)

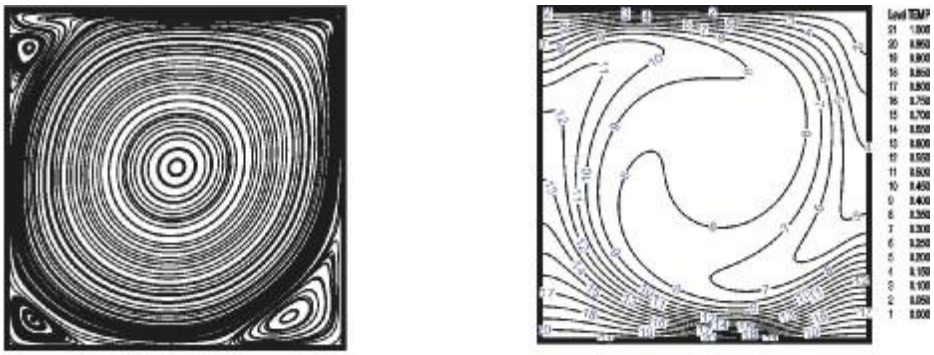

Pr = 0.1

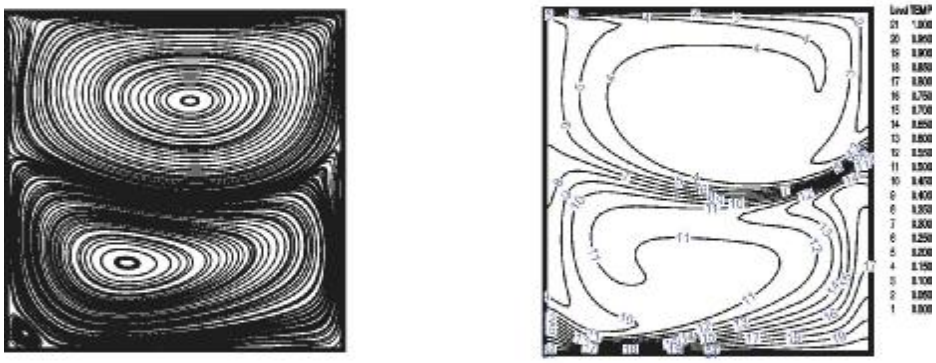

Pr = 1.0

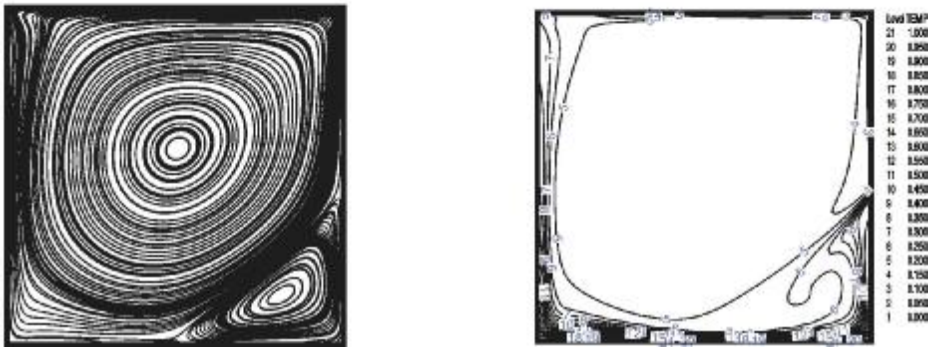

Pr=10.0

Streamlines **Isotherms**

Fig 6.11 Flow and temperature field in a cavity due to mixed convection for Re=1000 & Gr=10^6 (Ri=1.0)

(a) Re = 1000 , Ri = 0.0 ,Pr =1.0

(b) Re = 1000 , Ri = 0.1 ,Pr =1.0

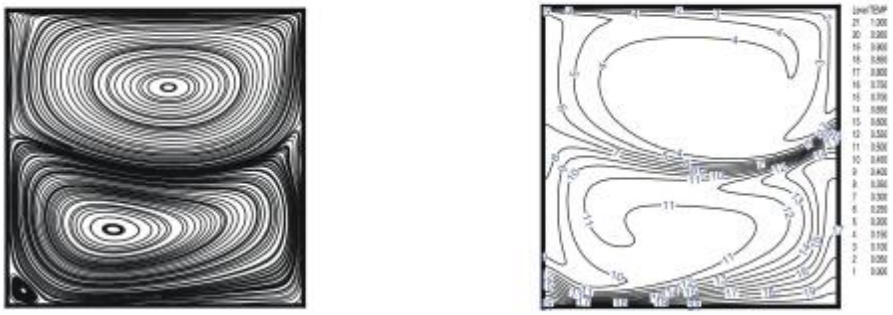

(c) Re = 1000 , Ri =1.0 ,Pr =1.0

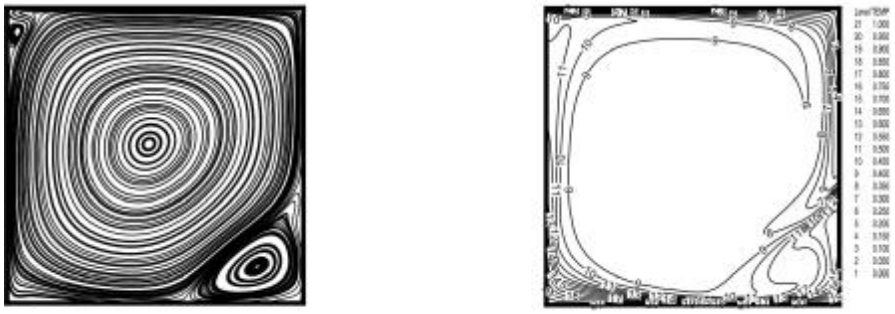

(d) Re = 1000 , Ri =10.0 ,Pr =1.0

Streamlines **Isotherms**

Fig 6.12 Streamlines Effect of Richardson number on flow and temperature field due to mixed convection in a square cavity

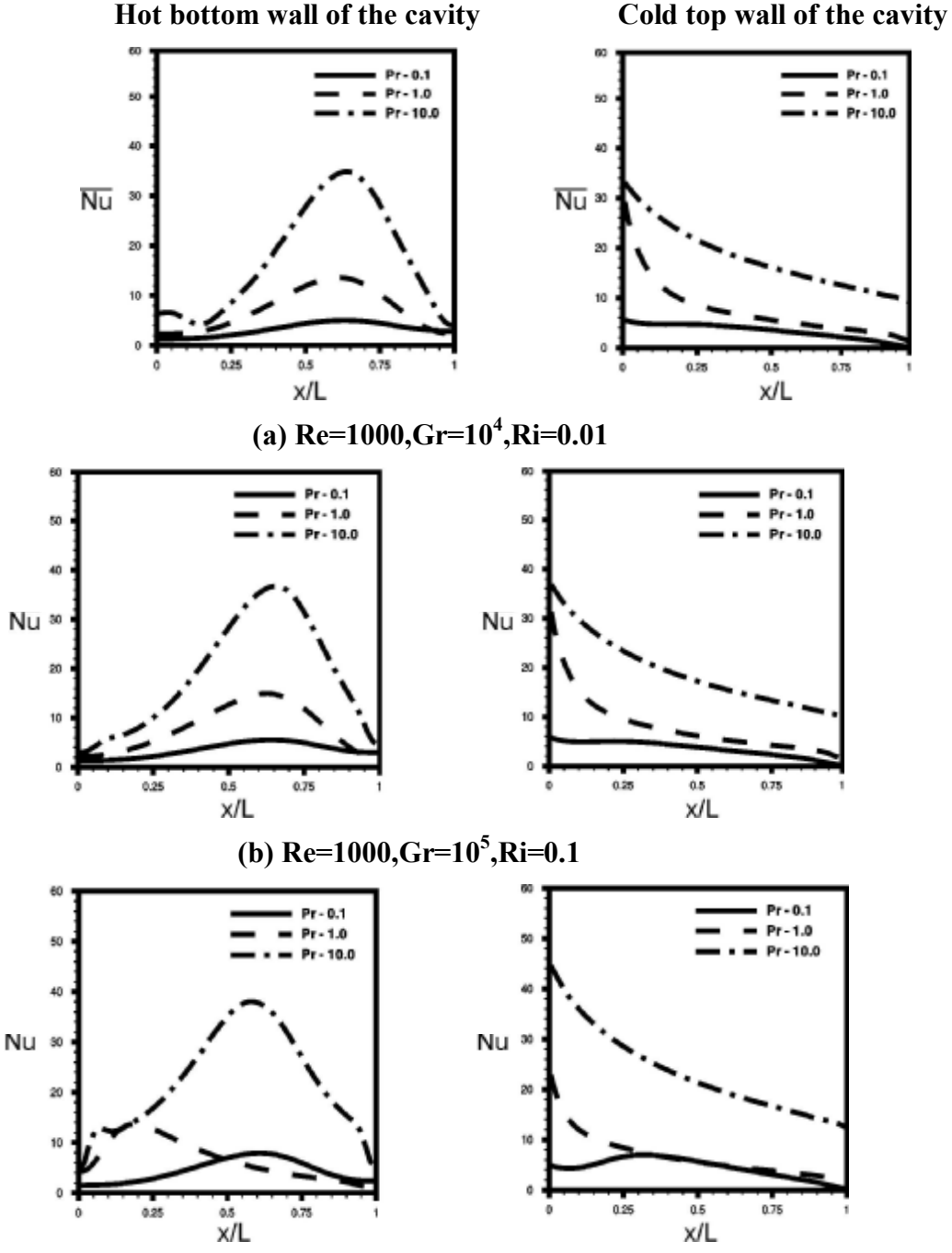

Fig 6.13 variation of local nusselt number along the top and bottom wall cavity

6.3.5 Correlation of the average Nusselt number to other parameters

Navier Stokes solution has been obtained in the present study for various combination of the parameters *Ri, Re* and *Pr* controlling the heat transfer in a bottom heated lid driven cavity. Now in case of mixed convection, part of the heat transfer is due to the forced convection and part due to free convection. Accordingly the Nusselt number can be expressed as $Nu_{mixed} = Nu_{forced} + Nu_{free}$. For the present problem, the forced convection due to the lid motion alone in absence of free convection, is controlled mainly by the boundary layers developed on the major portion of the hot floor of the cavity. However in the strictest sense, this heat transfer rate is eventually modified to considerable extent partly due to the stagnation effect of the impinging cold jet convected from the top and partly due to the recirculation effect of the DSE near the right bottom corner. If the forced convection is assumed to be controlled by the Reynolds number and Prandtl number only as in the case of boundary layer cooling of a hot flat plate, the Nusselt number may be expressed in the following form :

$$Nu_{forced} = A\,Re^{0.5}\,Pr^{0.33} \tag{6.1}$$

The free convective heat transfer due to thermal buoyancy, on the other hand, is decided by the Rayleigh and the Prandtl numbers. The average Nusselt number due to free convection for a differentially heated cavity may be expressed (Catton *et al (1967*) as :

$$Nu_{free} = B\left(Ra\,Pr/\left(0.2 + Pr\right)\right)^{0.25} \tag{6.2}$$

The total average Nusselt number for mixed convection may now be expressed as a simple summation of the forced and free heat transfer coefficients as following :

$$Nu_{mixed} = A\,Re^{0.5}\,Pr^{0.33} + B\left(Ra\,Pr/\left(0.2 + Pr\right)\right)^{0.25} \tag{6.3}$$

The constants *A* & *B* may be computed from a linear least square estimation from the set of nine data points obtained by CFD analyses ,over a range of *Ri* and *Pr* at *Re*=1000.

Fig. 6.14. shows the estimate line as well as the computation points obtained from CFD analyses. The intercept of the estimated line on the *y*- axis of the plot (A= 0.168) indicates the average Nusselt number for purely forced convection in a lid driven cavity when the value of *Ri* tends to zero, whereas the value of *A* for a simple thermal boundary layer on a flat plate is 0.332. This difference may be attributed to the gross difference in the flow pattern of a flat plate boundary layer and the complex flow pattern in the cavity. No definite

reason can be given to explain the scatter of the computation data. Perhaps the simple addition of the effects of forced and free convection does not correctly depict the complex non-linear interaction between the shear and the buoyancy forces in the flow and heat transfer. A better correlation needs more extensive computation over wider range of the control parameters.

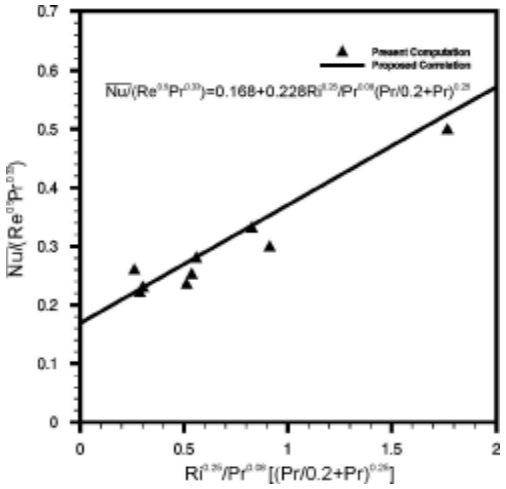

Fig 6.14 Correlation of average heat transfer coefficient with the operating parameters, for bottom heated lid driven cavity

CONCLUDING REMARKS

- The parameters which decide the flow and heat transfer in free and mixed convection in a differentially heated lid-driven rectangular cavity are identified from the non-dimensional governing conservation equations as : Lid velocity based Reynolds number (*Re*), Prandtl number (*Pr*), Grashof number (*Gr*) or the Richardson number ($Ri=Gr/Re^2$) and the cavity aspect ratio (*H/L*).

- Effect of Aspect Ratio for free convection in a bottom heated rectangular cavity is studied. The critical Rayleigh number for transition from conduction to convective mode for a cavity aspect ratio of 0.5 is correctly predicted and the experimentally observed Rayleigh-Benard convection cells are also captured reasonably well for cavity aspect ratios other than unity.

- The code RANS2D is used successfully for some of the parametric studies on the present problem of mixed convection in a bottom heated lid driven square cavity. Computations are carried out for four different Richardson number (Ri =0.01,0.1,1 and 10) and three different Prandtl number (Pr = 0.1, 1 and 10) for a given lid velocity based Reynolds number as 1000.

- Physically realistic flow pattern and temperature distribution are obtained for all the cases investigated and the physical quantities of engineering interest like local or average Nusselt number compare reasonably well with other computational values reported in literature for the same operating conditions.

- From the computed data on the different flow situations investigated, simple algebraic correlations have been established for the average Nusselt number as a function of other operating parameters like *Re, Ri* and *Pr* in case of mixed convection in a cavity. The forced convection is in all cases observed to be assisted or augmented by the free convection effects.

- Further parametric CFD analysis-based studies are required in future to arrive at more definite and reliable correlations to be used for heat transfer rate due to laminar mixed convection in a bottom heated lid driven cavity.

ACKNOWLEDGEMENT

The authors wish to express their heartfelt thanks to Dr M.D.Deshpande , Head CTFD Division for his very careful review of this document and his valuable suggestions and advice which improved the technical contents and the presentation of this work to a considerable extent.

REFERENCES

Bernard H. (1900), "Les Touribillions Cellularies Dans une Nappe Liquide," *Revue General des Sciences Pures et Appliquees*, vol. 11, pp. 1261-71

Catton I.,Edwards D.K.(1967), Effect of side walls on natural Convection between horizontal plates heated from below*, Journal of Heat Transfer, pp .295-299*

Chandrasekhar S. (1961), *Hydrodynamic and Hydromagnetic stability* , Oxford at the Clarendon Press, England, pp. 9-73

Clever R.M., Busse F.H (1974) Transition to Time-dependent Convection, Journal of Fluid Mechanics, vol.65, pp. 625-646

Eckert E.R.G., Carlson W.G. (1961), Natural Convection in an Air Layer Enclosed between two vertical Planes with Different Temperatures, *International Journal of Heat and Mass Transfer*, vol. 2, pp. 106-120

Elder J.W (1965), Laminar Free Convection in an Vertical Slot, *Journal of Fluid Mechanics.,* vol. 23, pp. 77-98

Fathima A., Baldawa N.S., Pal, S., Majumdar, S.(1994), Grid generation for arbitrary 2D configurations using a differential algebraic hybrid method, *NAL PD CF 9416*

Gebhart B. (1971), *Heat transfer* , 2nd ed. McGraw-Hill, New York, pp. 388-397

Ghia U., Ghia K.N., Shin C.T. (1982), High-Re Solutions for Incompressible Flow Using the Navier-Stokes Equations and a Multigrid Method, *Journal of Computational Physics,* vol. 48, pp. 387-411

Koseff J.R., Street R.L., Gresho P.M., Upson C.D.,Humprey J.A.C.,To W.M. (1983), *Proceedings 3rd International Conference on Numerical Methods in Laminar and Turbulent Flow,* University of Washington, pp. 564-581, August 8th -11th

Kulkarni D. S., Rajani B. N., Majumdar, S. (2001), Studies on temporal and spatial discretisation schemes used in a Pressure-based RANS algorithm for incompressible flow. *NAL PD CF 0108*

Leonard B. P.(1979), A stable and accurate convective modeling procedure based on quadratic interpolation, *Computer Methods in Applied Mechanics Engineering*, vol. 19, pp.59-98

Majumdar S. (1988), Role of underrelaxation in momentum interpolation for calculation of flow with non-staggered grids, *Numerical Heat Transfer*, vol.13, pp. 125-132

Majumdar S., Rajani B.N., Kulkarni D. S., Mohan Sripathi. (2003), RANS Computation of Low Speed Turbulent Flow in Complex Configuration. *Proc., State of the Art and Future Trends of CFD at NAL, NAL SP 0301*, pp. 31-48

Moallemi M.K., Jang K.S.(1992), Prandtl number effects on laminar mixed convecton heat transfer in a lid-driven cavity. *International Journal of Heat and Mass Transfer*, vol. 35, No. 8, pp. 1881-1892

Mohamad A., Viskanta R.(1993), Flow and thermal structures in a lid-driven cavity heated from below. *Fluid Dynamics Research*, vol. 12, pp. 173-184

Morozov G.V.,Motorin O.V., Shishkova N.A.(2001), Mixed convection of water in a rectangular lid-driven cavity, *3rd AFOSR International Conference on Direct Numerical Simulation and Large Eddy Simulation (TAICDL)* , University of Texas at Arlington.

Ostrach S.(1954), Combined Natural and Forced – Convection laminar flow and heat transfer of fluids with and without heat sources in channels with linearly varying wall temperatures .*National Advisory Committee for Aeronautics*, *TN 3141*

Prasad A.K., Koseff J.R.(1989), Heat Transfer in Convective Flows, *HTD-107*, pp.155-162, ASME, New York

Prasad A.K., Koseff J.R.(1996), Combined forced and natural convection heat transfer in a deep lid-driven cavity flow, *International Journal of heat and fluid flow*, vol. 17, pp. 460-467

Patankar S.V., Spalding D.B. (1972) A calculation for heat, mss and momentum transfer in three dimensional parabolic flows, *International Journal of Heat and Mass Transfer,* vol. 15, pp. 1778-1806

Patankar S.V (1980), *Numerical Heat Transfer and Fluid Flow*, Hemisphere Pub. Co.

Rayleigh Lord. (1916), "Convectve Currents in a Horizontal Layer of Fluid When the Higher Temperature Is on the Underside,; *Philosophical Magazine* , vol. 2, pp. 529-546

Rubel Arthur., Fred Landis (1969), Numerical Study of Natural Convection in a Vertical Rectangular Enclosure, *The Physics of Fluids Supplement II ,208*

Vahl Davis G. de., Mallinson G.D. (1973), The method of the false transient for the solution of coupled elliptic equations, *Journal of Computational Physics*., vol. 12, pp. 435-461

Wan D.C., Patnaik B.S.V., Wei G.W (2001), A new benchmark solution for the buoyancy-driven cavity by discrete singular convolution. *Numerical Heat Transfer*, Part B, vol. 40, pp. 199-228

Vahl Davis G. de., Mallinson, G.D. (1976), An Evaluation of upwind and central difference approximations by a steady of re-circulating flow*, Computers and Fluids*, vol. 4, pp. 29-43

Vahl Davis G. de (1983), Natural convection of air in a square cavity: A bench mark numerical solution, , *International Journal for Numerical Methods in Fluids*, vol. 3, pp. 249-264

Xu Kun ., Lui Shiu Hung .(1998), Rayleigh-Benard Simulation using Gas-kinetic BGK Scheme in the Incompressible Limit, *ICASE Report No. 98-56*, NASA Langley Research Center, Hampton, Virginia

NATIONAL AEROSPACE LABORATORIES	DOCUMENTATION SHEET Class : Unrestricted No. of copies : 30

Title	:	Laminar Mixed Convective heat transfer in a bottom heated lid driven square cavity	
Author(s)	:	D.S.Kulkarni, N.Mahendran, Sekhar Majumdar	
Division	:	CTFD	NAL Project No. : C-9-000
Document No.	:	PD CF 0503	Date of issue : January 2005

Contents : 40 Pages | 18 Figures | - Tables | 29 References

External Participation : Second author is a Post-graduate student from Sri Venkateswara College of Engineering , Sriperumbudur

Sponsor	:	Nil
Approval	:	Head, CTFD Division
Remarks	:	Nil
Keywords	:	Navier Stokes solver, Cartesian grid, low diffusive high order upwind scheme, free convection in square cavity and cylindrical annulus, laminar slot jet impingement on a hot plate

Abstract :

The present work focuses on a detailed CFD analysis of two dimensional laminar incompressible flow and heat transfer in a rectangular enclosure for which the top lid wall, maintained at a lower temperature, is either stationary (free convection) or driven parallel to itself at a uniform speed (mixed convection) where as the other three walls are stationary, the two vertical walls are thermally insulated and the horizontal bottom wall is maintained at a higher temperature from an external heat source. The computations are carried out using an implicit second order accurate finite volume Navier Stokes solver based on pressure-velocity solution strategy with cartesian grid, cartesian velocities and collocated variable arrangement. The flow pattern and temperature distribution are compared to available measurement and computation data.

LAMINAR MIXED CONVECTIVE HEAT TRANSFER IN A BOTTOM HEATED LID DRIVEN SQUARE CAVITY

D.S.Kulkarni N. Mahendran Sekhar Majumdar

NAL PDCF 0503

Computational and Theoretical Fluid Dynamics Division
National Aerospace Laboratories, Bangalore 560 017

January 2005